Check for updates

JGR Atmospheres

RESEARCH ARTICLE
10.1029/2026JD046327

Meteorological and Emission Drivers of Compound Heat and Ozone Pollution Episodes in Oklahoma City During Periods Influenced by Atlantic Tropical Cyclones

Xiao-Ming Hu[1,2], Chenghao Wang[2,3], Siqi Ma[4], Daniel Tong[4,5], Ming Xue[1,2], and Adriana E. Larrea Valdivia[6]

[1]Center for Analysis and Prediction of Storms, University of Oklahoma, Norman, OK, USA, [2]School of Meteorology, University of Oklahoma, Norman, OK, USA, [3]Department of Geography and Environmental Sustainability, University of Oklahoma, Norman, OK, USA, [4]Department of Atmospheric, Oceanic and Earth Sciences, George Mason University, Fairfax, VA, USA, [5]Center for Satellite and Earth Science Research, George Mason University, Fairfax, VA, USA, [6]Departamento Académico de Química, Centro de Investigación Aplicada y Laboratorios Especializados (CIALE), Universidad Nacional de San Agustín de Arequipa, Arequipa, Perú

Key Points:

- Compound heat and O_3 pollution episodes in Oklahoma stem from atypical weather, revealed by observations and sub-km WRF-Chem simulations
- Southwestward transport of pollutants from the Tulsa area and weak prefrontal winds drive O_3 buildup over Oklahoma City
- NO_x emissions from the Tulsa metropolitan area contributed to ~10 ppbv of O_3 in Oklahoma City during the 15 June 2021 compound event

Correspondence to:
C. Wang and X.-M. Hu,
chenghao.wang@ou.edu;
xhu@ou.edu

Citation:
Hu, X.-M., Wang, C., Ma, S., Tong, D., Xue, M., & Larrea Valdivia, A. E. (2026). Meteorological and emission drivers of compound heat and ozone pollution episodes in Oklahoma City during periods influenced by Atlantic tropical cyclones. *Journal of Geophysical Research: Atmospheres*, *131*, e2026JD046327. https://doi.org/10.1029/2026JD046327

Received 5 JAN 2026
Accepted 22 AUG 2026

Author Contributions:
Conceptualization: Xiao-Ming Hu, Ming Xue, Adriana E. Larrea Valdivia
Investigation: Xiao-Ming Hu
Methodology: Xiao-Ming Hu, Siqi Ma, Daniel Tong
Writing – original draft: Xiao-Ming Hu
Writing – review & editing: Chenghao Wang

© 2026 The Author(s). Journal of Geophysical Research: Atmospheres published by Wiley Periodicals LLC on behalf of American Geophysical Union. This is an open access article under the terms of the Creative Commons Attribution License, which permits use, distribution and reproduction in any medium, provided the original work is properly cited.

Abstract Compound heat and ozone (O_3) pollution events are widespread and pose significant health risks in urban areas. In the Southern Great Plains (SGP), where heat waves are becoming more frequent and intense, these compound events represent a growing environmental and public health concern, underscoring the need for improved process-based understanding to support effective risk assessment and mitigation. This study investigates the three severe O_3 pollution episodes recorded in Oklahoma City (OKC) since 2014–19 July 2018 (106 ppb), 15 June 2021 (93 ppb), and 6–7 August 2024 (86 ppb)—with a particular focus on the June 2021 event that coincided with a pronounced heat wave. Using high-resolution WRF-Chem simulations, we examine the formation mechanisms and identify key meteorological and emission-related contributors to the episode. The episode developed under atypical summer conditions over the SGP, characterized by a frontal passage coincided with the evolution of a tropical storm over the Atlantic Ocean. TROPOMI-based satellite observations reveal substantial power plant emissions in addition to urban emissions in the Tulsa region. Under persistent northeasterly winds, southwestward transport of pollutants from Tulsa on 14–15 June supplied additional pollutants to OKC. Meanwhile, the weak-wind zone over OKC on 15 June, ahead of the advancing front, further favored pollutant accumulation and O_3 production. WRF-Chem sensitivity experiments illustrate that total NO_x emissions from the Tulsa area contributed ~4–15 ppbv of surface O_3 in OKC on 15 June 2021, while power plants alone accounted for ~2–6 ppbv, with contributions varying by location.

Plain Language Summary In the Southern Great Plains, heat waves are becoming more frequent and intense, increasing the risk of concurrent extreme heat and unhealthy ozone (O_3) pollution events. These compound events can pose serious health risks. This study focuses on an extreme O_3 pollution event that occurred in Oklahoma City (OKC) on 15 June 2021 during a heat wave. Using high-resolution WRF-Chem simulations, we examine why O_3 levels became unusually high and identify the key meteorological patterns and emission sources involved. We find that this event developed under unusual summer weather conditions, including the passage of a front linked to the formation of a tropical storm over the Atlantic Ocean. Winds transported pollutants from the Tulsa area toward OKC, while weak winds on 15 June allowed pollutants to build up and O_3 to form efficiently, which collectively contributed up to 15 ppbv of O_3 in OKC. In contrast, our results show that extreme O_3 pollution in OKC is unlikely during typical summer conditions, when southerly winds promote better dispersion. This study highlights how rare combinations of weather patterns and regional emissions can trigger dangerous heat and air pollution extremes, and offers insights that could help guide more targeted air quality management strategies.

1. Introduction

Heat waves and O_3 pollution are two major health threats that are increasingly intertwined with global warming. Since high temperature enhances O_3 formation, heat wave and O_3 pollution are strongly coupled. When heat wave and O_3 pollution occur simultaneously, they pose a greater public threat than either stressor alone, leading to elevated mortality and morbidity (Analitis et al., 2014; Du et al., 2024; Feron et al., 2023). Such periods are defined as compound heat and O_3 pollution episodes (Zscheischler et al., 2020). A recent multi-decadal analysis

21698996, 2026, 17, Downloaded from https://agupubs.onlinelibrary.wiley.com/doi/10.1029/2026JD046327 by University Of Oklahoma, Wiley Online Library on [12/10/2026]. See the Terms and Conditions (https://onlinelibrary.wiley.com/terms-and-conditions) on Wiley Online Library for rules of use; OA articles are governed by the applicable Creative Commons License

shows that such compound events are more frequent and intense in about 90% of U.S. cities compared to their rural surroundings, a phenomenon driven by the complex interplay between meteorology, emissions, and land–atmosphere processes (Wang, Hu, et al., 2025). Future climate projections suggest warmer conditions with decreased cloud cover and more frequent stagnation periods, which are conducive to elevated O_3 levels and are likely to increase the occurrence of compound heat and O_3 pollution episodes in the U.S. (Fang et al., 2013; Jacob & Winner, 2009). Despite the high frequency of such compound events in the U.S. (Wang, Hu, et al., 2025), the understanding, quantification, and prediction of such events still remain limited. Therefore, improved understanding and modeling of these compound events are essential for strengthening risk assessment and informing mitigation strategies (Zscheischler et al., 2020).

The Southern Great Plains (SGP), comprising Texas, Oklahoma, and Kansas, is particularly susceptible to heat waves (Hoerling et al., 2013; Lee et al., 2016; Namias, 1982; Yang et al., 2019) and is projected to experience further increases in the frequency, intensity, and duration of heat waves under future climate conditions (Lau & Nath, 2012; Perkins-Kirkpatrick & Lewis, 2020; Teng et al., 2016). Extreme heat in the SGP is strongly modulated by large-scale circulation anomalies, including persistent upper-level ridging, suppressed convective activity, and soil moisture–temperature feedbacks, with the region recognized as one of the global hotspots of land–atmosphere coupling that amplifies heat-wave intensity and persistence (Koster et al., 2004; Seneviratne et al., 2010). According to the Köppen–Geiger climate classification, the SGP spans a pronounced east–west transition from humid subtropical in eastern Texas and Oklahoma to semi-arid steppe climate toward western Oklahoma and the Texas Panhandle, suggesting strong gradients in moisture availability and land–atmosphere coupling (Beck et al., 2018). Future climate projections indicate a poleward and eastward expansion of drier and warmer climate regimes across the central U.S., with semi-arid and hot climate zones encroaching into regions historically characterized by more humid conditions (Beck et al., 2018; Cui et al., 2021). These projected changes imply more frequent hot extremes, reduced evaporative cooling, and an increased likelihood of meteorological conditions conducive to compound heat-related hazards.

Despite the implementation of emission-control regulations over the past several decades (McDonald et al., 2018; Shapiro, 2022), lower-tropospheric O_3 pollution remains a recurring issue in the south-central U.S. The U.S. National Ambient Air Quality Standard (NAAQS) for ground-level O_3, that is, a daily maximum 8-hr average of 70 ppbv, is frequently exceeded in the region (Choi & Souri, 2015; Hu et al., 2019; Pongprueksa, 2013; Qin et al., 2007; Sather & Cavender, 2012). It is noteworthy that to better protect public health, the World Health Organization (WHO) recommends a more stringent guideline of 100 μg m^{-3} (~50 ppbv) for the daily maximum 8-hr mean O_3, a threshold that is increasingly adopted by air quality assessments in many countries (Feron et al., 2023; Meng et al., 2022; Wang, Hu, et al., 2025; World Health Organization, 2021). In a warmer future, compliance with such stringent O_3 targets might become increasingly challenging. Air pollutant emissions in the U.S. have decreased dramatically over the past few decades preceding 2019. National statistics show that emissions of volatile organic compounds (VOCs), NO_x, CO, SO_2, and particulate matter declined by approximately 24%–90% between 2000 and 2023, depending on the species (https://www.epa.gov/air-trends/air-quality-national-summary). These reductions have led to widespread improvements in ambient air quality; however, decreases in surface O_3 have been more modest and spatially heterogeneous compared to those of other primary pollutants (Shapiro, 2022). Moreover, recent studies indicate that the reduction in NO_x emissions has shifted many U.S. urban areas from NO_x-saturated to NO_x-limited or transitional regimes (Jin et al., 2020), increasing the responsiveness of surface O_3 to changes in NO_x emissions and regional transport of these sources. It is noteworthy that summertime O_3 exceedances have been documented in major metropolitan areas over the SGP such as Houston, Dallas-Fort Worth (DFW), and OKC (Hu, 2008; Hudak, 2014; Kim, Byun, & Cohan, 2009; Ramsey et al., 2014).

In summer, westward extension of the Bermuda subtropical high favors the development of a southerly low-level jet (LLJ) over the SGP, while transient synoptic processes (e.g., passages of frontal systems) may disturb such flow patterns at times (Klein et al., 2015; Lei et al., 2018; Zhu & Liang, 2013). Interannual variations in the Bermuda high have been linked to measurable changes in summer-mean surface O_3. A stronger/weaker Bermuda high can lead to lower/higher summer mean O_3 changes on the order of ~6 ppbv in this region (Zhu & Liang, 2013), likely because a stronger Bermuda high can strengthen southerly geostrophic winds and moisture transport from the Gulf of Mexico, leading to better ventilation and reduced potential for extreme O_3 accumulation (Hu et al., 2019; Sumner, 2025). Some recent studies illustrate that frontal systems play a critical role in the formation of some severe O_3 pollution episodes in the SGP (Lei et al., 2018, 2019). The stagnant conditions

21698996, 2026, 17, Downloaded from https://agupubs.onlinelibrary.wiley.com/doi/10.1029/2026JD046327 by University Of Oklahoma, Wiley Online Library on [12/10/2026]. See the Terms and Conditions (https://onlinelibrary.wiley.com/terms-and-conditions) on Wiley Online Library for rules of use; OA articles are governed by the applicable Creative Commons License

within the convergence zone ahead of the fronts sometimes lead to the accumulation of primary pollutants and subsequent formation of severe O_3 pollution, as documented for the DFW metropolitan area. Some of such frontal systems were influenced by passages of tropical cyclones over eastern U.S. coast or the Atlantic Oceans (Hu et al., 2019). Whether similar front-related weather patterns can trigger severe O_3 pollution episodes in Oklahoma remains to be examined.

A few large field experiments, including the Texas Air Quality Studies in 2000 (TexAQS2000) (Daum et al., 2004; Jiang & Fast, 2004; Wert et al., 2003) and 2006 (TexAQS II) (Langford et al., 2011; Parrish et al., 2009; Senff et al., 2010; Yu et al., 2012), as well as aircraft measurements in August 2005 (Luria et al., 2008), have been conducted to investigate O_3 formation mechanisms in Texas (Zhang et al., 2013; Zhang & Ying, 2011). These efforts have substantially advanced the understanding of O_3 chemistry, emissions, and meteorological controls in major Texas metropolitan areas, particularly Houston and DFW. In comparison, O_3 pollution and compound heat and O_3 hazards in Oklahoma have received much less attention. Limited O_3 studies over Oklahoma have mainly focused on nighttime secondary O_3 maxima and related nocturnal boundary layer processes (Hu, Klein, Xue, Shapiro, & Nallapareddy, 2013; Hu, Klein, & Xue, 2013; Klein et al., 2010, 2014). One statistical study focused on O_3 climatology in Oklahoma and concluded that hot and dry conditions lead to O_3 exceedance days and extended exposure risks for both human and vegetation (Ramsey et al., 2014). However, the formation mechanism of severe compound heat and O_3 pollution events in Oklahoma remains unexplored.

The OKC area spanned ~1,610 km^2 with a population of ~1 million in 2025, placing it among the top 10 largest U.S. cities by land area. Urban heat island effects have been well documented in OKC (Basara et al., 2008; Hu, Klein, Xue, Lundquist, et al., 2013; Hu et al., 2016), which may potentially enhance O_3 formation (Gamarro et al., 2026; Han et al., 2022). Despite long-term declines in air pollutant emissions across much of the U.S., recent years have seen increasing concerns regarding O_3 pollution in Oklahoma. According to the Oklahoma Department of Environmental Quality (DEQ), there were 14 days in 2024 when the 8-hr average O_3 concentration exceeded the NAAQS of 70 ppbv in OKC (https://applications.deq.ok.gov/webdata/aqd/monitoring/charts/OKCAQI2024.htm), representing one of the highest levels of O_3 pollution in recent years. Meanwhile, emissions of nitrogen oxides ($NO_x = NO + NO_2$) from Electric Generating Units (EGUs) over Oklahoma increased from 16,000 tons in 2019 to 21,000 tons in 2024, including a 12.6% increase between 2023 and 2024 alone. In addition, rapid expansion of energy-intensive infrastructure, particularly data centers, is expected to substantially increase regional electricity demand, potentially leading to further increases in EGU emissions in the future. These trends raise concerns regarding the role of power plant emissions in worsening O_3 pollution over Oklahoma. It is noteworthy that a few large power plants reside within 200 km of OKC, including three in the Tulsa region ~150 km to the northeast, that is, the Muskogee, Grand River, and Northeastern power plants (see their locations in Figure 1b). These facilities are either coal-fired or use a combination of coal, natural gas, and oil. Power plant emissions, particularly NO_x, have been shown to play an important role in O_3 exceedance in eastern U.S. (Fibiger et al., 2018; Frost et al., 2006; Nunnermacker et al., 2000; Senff et al., 1998; Trainer et al., 1995), Texas (Brown et al., 2012; Hu et al., 2019; Kim et al., 2011), and western U.S. (Kim, Heckel, et al., 2009). However, their role in O_3 pollution in Oklahoma remains poorly understood. While Rozhina et al. (2021) investigated aerosol emissions and associated health impacts from the Muskogee power plant, the implications for O_3 pollution were not addressed. Furthermore, the combined influence of power plant emissions and urban emissions from the Tulsa metropolitan area on O_3 pollution in OKC has never been systematically investigated previously. Addressing these gaps is important for better understanding the formation mechanisms of compound heat and O_3 pollution events in this region.

Importantly, resolving the influence of these regional emission sources on O_3 formation requires numerical models that can accurately represent near-source chemistry, dilution, and downwind transport. High-resolution satellite data show that NO_x emitted from point sources can be rapidly titrated and diluted down to near-background levels within only a few kilometers through chemistry and dispersion (Jin et al., 2025). Coarse-resolution chemical transport models may therefore distort the NO_x–O_3 chemistry (Gillani & Pleim, 1996), particularly in the downstream regions of point sources such as power plants. Operational real-time air quality forecasts over the U.S. by the National Air Quality Forecast Capability (NAQFC) use a ~13 km horizontal grid spacing (Huang et al., 2025; Lee et al., 2017), a resolution also used by some recent air quality simulations (Ma et al., 2025). Such resolutions may be too coarse to adequately resolve the impacts of power plant emissions on O_3 formation (Lawal et al., 2022), particularly within the ~200 km corridor between Tulsa and OKC, where various processes interact on much smaller spatial scales.

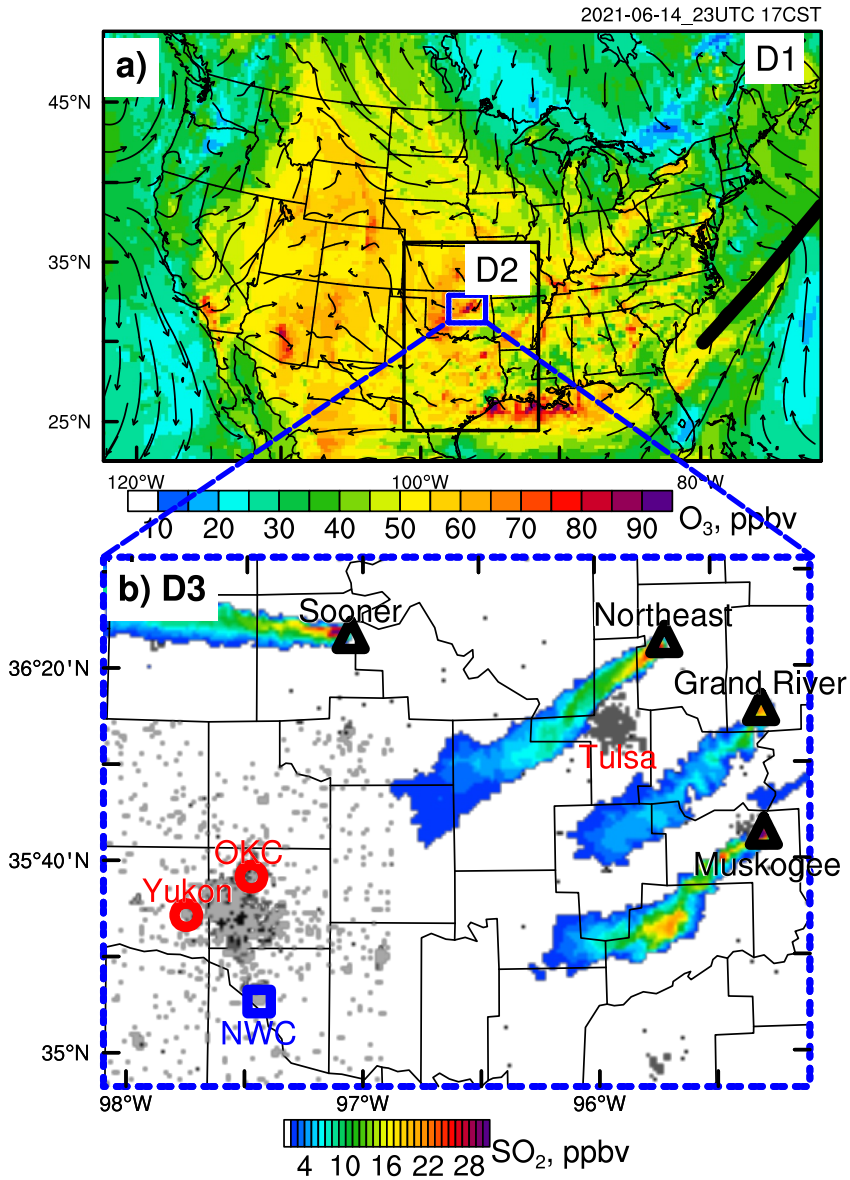


Figure 1. (a) Simulated O_3 and wind fields in the 1st domain by the control WRF-Chem experiment on 14 June 2021. The nested domains 2 (D2) and 3 (D3), and track of tropical storm Bill over the Atlantic Ocean are marked. (b) Simulated SO_2 in D3. The four power plants, two EPA O_3 sites at OKC and Yukon, and the National Weather Center (NWC) ozonesonde launching site are marked with triangles, circles, and square respectively. The urban land-use is shaded in gray.

In this study, sub-kilometer resolution simulations using the Weather Research and Forecasting model coupled with Chemistry (WRF-Chem, Fast et al., 2006; Grell et al., 2005; Skamarock & Klemp, 2008) are conducted over Oklahoma for the first time to examine two of the compound heat and O_3 pollution events in the SGP that occurred during 15–16 June 2021 and 6–7 August 2024, with the analysis focusing primarily on the former. Notably, both episodes coincided with the passage of Atlantic tropical cyclones (Bill in 2021 and Debby in 2024), suggesting a potential role of cyclone-associated synoptic conditions in shaping meteorological environments favorable for severe O_3 pollution. The simulations are designed to quantify the impacts of emissions from power plants and Tulsa metropolitan area on O_3 pollution in OKC, as well as the associated meteorological mechanisms driving these events. The June 2021 episode is accompanied by a comprehensive set of unique observations, including surface meteorological and O_3 data, satellite retrievals, and ozonesonde profiles, offering a valuable opportunity to investigate the underlying physical and chemical processes and to fully evaluate the model's performance. The

21698996, 2026, 17, Downloaded from https://agupubs.onlinelibrary.wiley.com/doi/10.1029/2026JD046327 by University Of Oklahoma, Wiley Online Library on [12/10/2026]. See the Terms and Conditions (https://onlinelibrary.wiley.com/terms-and-conditions) on Wiley Online Library for rules of use; OA articles are governed by the applicable Creative Commons License

21698996, 2026, 17, Downloaded from https://agupubs.onlinelibrary.wiley.com/doi/10.1029/2026JD046327 by University Of Oklahoma, Wiley Online Library on [12/10/2026]. See the Terms and Conditions (https://onlinelibrary.wiley.com/terms-and-conditions) on Wiley Online Library for rules of use; OA articles are governed by the applicable Creative Commons License

findings of this study are expected to inform strategies for reducing human and vegetation exposure during similar compound heat and O_3 pollution episodes in other cities with similar settings.

The rest of this paper is organized as follows. Section 2 describes the selected air pollution episodes, observational data sets, and design of WRF-Chem simulations. Section 3 examines the contributing factors for the events through control and sensitivity simulations. Finally, Section 4 contains a summary and discussion of the main findings.

2. Data, Model Configuration, and Numerical Experiment Design

2.1. Overview of the Compound Heat and O_3 Pollution Episodes

Three severe compound heat and O_3 pollution episodes potentially influenced by Atlantic tropical cyclones were identified over Oklahoma based on long-term observations, including 15–16 June 2021 during the passage of Tropical Storm Bill, 6–7 August 2024 during Hurricane Debby, and 19 July 2018, which occurred just 2 days after Hurricane Beryl. Detailed WRF-Chem simulations were conducted for the June 2021 and August 2024 events, with the analysis focusing primarily on the June 2021 episode. As mentioned in Section 1, this event is accompanied by a unique and comprehensive set of observations, providing an exceptional opportunity to investigate the underlying physical and chemical processes and rigorously evaluate model performance. The August 2024 event is primarily included as a supporting case to examine the robustness and broader applicability of the identified mechanisms.

From 14 to 16 June 2021, Tropical Storm Bill tracked off the U.S. eastern coast over the Atlantic Ocean (Figures 1a and 2b). Meanwhile, a synoptic frontal system moved across the SGP. Ahead of the advancing front, a compound heat and O_3 pollution episode developed over the region during 15–16 June 2021. In OKC, the maximum hourly O_3 concentration reached 93 ppbv on 15 June, while widespread O_3 pollution was observed across the DFW metropolitan area, where hourly O_3 levels approached 128 ppbv on 16 June. Satellite observations from MODIS indicate predominantly clear-sky conditions over Oklahoma during 14–16 June 2021, with only thin, scattered clouds over parts of Texas on Jun 15 (not shown), which favored strong solar radiation and efficient photochemical O_3 production.

This high O_3 level coincided with a multi-day heat wave spanning from 15 June to 18 June 2021. Following previous studies (Leffel et al., 2025; Wang, Hu, et al., 2025), the heat wave is defined using a city-scale, spatially averaged metric rather than observations from a single weather station. Specifically, daily mean near-surface air temperature averaged across the entire OKC area exceeded the 90th percentile threshold of a 30-year (1981–2010) climatology of the rural surroundings for four consecutive days. Both the temperature time series and the 30-year climatology were based on a reconstructed temperature data set that incorporates Daymet v4.1 data (Thornton et al., 2021) bias-corrected through a modified quantile delta mapping method to account for the urban heat island effect (Wang, Hu, et al., 2025). Daily percentile thresholds were calculated within a 15-day moving window centered on each calendar day.

While the heat wave conditions are identified based on near-surface air temperature, the synoptic-scale circulation plays a critical role in modulating pollutant transport and accumulation. In particular, the convergence zone and weak flow environment over Oklahoma on 15 June 2021 and 7 August 2024 (Figure 3) highlight the dynamic conditions that limited dispersion and promoted the buildup of O_3 and its precursors. This combination of sustained heat, clear skies, and anomalously weak ventilation provides a physically consistent framework for the development of the compound heat and O_3 pollution episodes examined in this study.

2.2. Observational Data Sets for NO_2, O_3, and Meteorology

Satellite remote-sensing data are first used to understand the regional-scale distributions of pollutants during this event. The Tropospheric Monitoring Instrument (TROPOMI) onboard the European Space Agency's Sentinel-5 Precursor (S5P) satellite has proven to be a valuable tool for studying NO_2 emissions and distribution (Xing et al., 2024). TROPOMI is a hyperspectral spectrometer that images the atmosphere with an overpass time of ~13:30 local time (LT) and a nadir spatial resolution of 3.5 km × 5.5 km. To ensure data quality, TROPOMI tropospheric column NO_2 (XNO_2) data were first filtered based on the retrieval quality assurance (QA) value, removing pixels with a QA value <0.75 following previous studies (e.g., Goldberg et al., 2024). This step

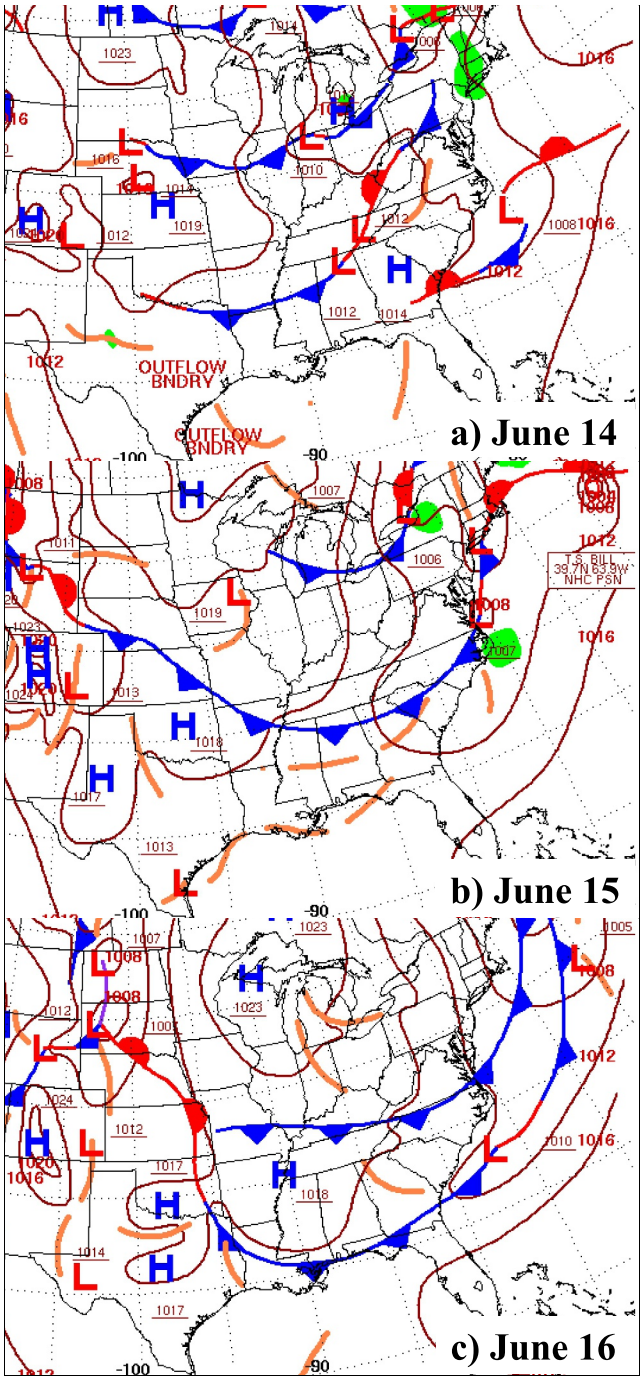


Figure 2. Weather maps at 1200 UTC on (a) 14, (b) 15, and (c) 16 June 2021, which were produced by the Weather Prediction Center of the National Centers for Environmental Prediction (http://www.wpc.ncep.noaa.gov/dailywxmap/).

accounted for potential contamination in the retrievals stemming from bright surfaces, presence of clouds, and solar geometries.

In addition, TROPOMI XNO_2 retrievals are sensitive to the assumed NO_2 vertical profiles used in the air mass factor (AMF) calculation, which is based on a priori profiles from the global Tracer Model 5 (TM5) at a coarse resolution ($1° \times 1°$). To reduce inconsistencies between satellite observations and our model simulations, we corrected the TROPOMI XNO_2 using a new tropospheric AMF (AMF_c) calculated based on the NO_2 vertical profiles simulated by WRF-Chem and TROPOMI's tropospheric averaging kernels (K). Following Li et al. (2021), the corrected $XNO_{2,c}$ is computed as:

$$XNO_{2,c} = \frac{AMF}{AMF_c} \cdot XNO_2 \quad (1)$$

$$AMF_c = \frac{AMF \sum_1^n NO_{2,i} \cdot K_i}{\sum_1^n NO_{2,i}} \quad (2)$$

$$K_i = \frac{AMF_{total}}{AMF} \cdot K_{total,i} \quad (3)$$

where $XNO_{2,c}$ is the corrected XNO_2 using WRF-Chem-based NO_2 vertical profiles ($NO_{2,i}$ in the i-th layer) interpolated to the TM5 vertical coordinate; $K_{total,i}$ and K_i are the total and tropospheric averaging kernels for the i-th layer from a prior TM5 model as provided in the TROPOMI data; AMF_{total} and AMF are the total and tropospheric AMF also from a prior TM5 model; and n is the tropopause layer index. Such a correction has been shown to enhance TROPOMI XNO_2 by as much as 60% near major emission sources and notably improve model–satellite agreement (Goldberg et al., 2021; Lawal et al., 2022; Ma et al., 2025).

Surface O_3 data are recorded hourly at EPA Air Quality System (AQS) ground-based monitoring sites around urban areas (Gao et al., 2022). In this study, O_3 data from the OKC and Yukon EPA sites (see their locations in Figure 1b) are analyzed, where O_3 extremes were measured during the selected episodes. Vertical O_3 structure during the event is based on ozonesonde observations launched on 16 June 2021 at the National Weather Center in Norman, Oklahoma (see its location in Figure 1b), ~35 km south of the OKC O_3 site. Although these soundings were originally designed to sample upper air impacted by convections in preceding days (Auth & Homeyer, 2023), they coincided with the compound heat and O_3 pollution event in this study. The ozonesonde profile on the afternoon of Jun 16 is used to examine the boundary layer O_3 structure following the severe O_3 day on 15 June in OKC.

Radiosonde Replacement System (RRS) sounding data are employed to assess boundary-layer structure, consistent with previous boundary-layer studies (e.g., Hu & Xue, 2016; Hu et al., 2020, 2023). The sounding data in BUFR format have a 1-s temporal resolution (i.e., one measurement per second) and are decoded and sampled at significant levels using NOAA-provided software (available at https://www.ncei.noaa.gov/data/us-radiosonde-bufr/doc/). The RRS sounding data are collected at the standard synoptic times of 1200 UTC (0600 CST) and 0000 UTC (1800 CST). Additional sounding data from the SGP Atmospheric Radiation Measurement (ARM) site in northern Oklahoma (downloaded from http://dx.doi.org/10.5439/1021460) are also utilized.

In addition, surface observations from the Oklahoma statewide mesoscale observing network (Mesonet) are used for model evaluation and examining meteorological conditions. The Oklahoma Mesonet consists of 120

21698996, 2026, 17, Downloaded from https://agupubs.onlinelibrary.wiley.com/doi/10.1029/2026JD046327 by University Of Oklahoma, Wiley Online Library on [12/10/2026]. See the Terms and Conditions (https://onlinelibrary.wiley.com/terms-and-conditions) on Wiley Online Library for rules of use; OA articles are governed by the applicable Creative Commons License

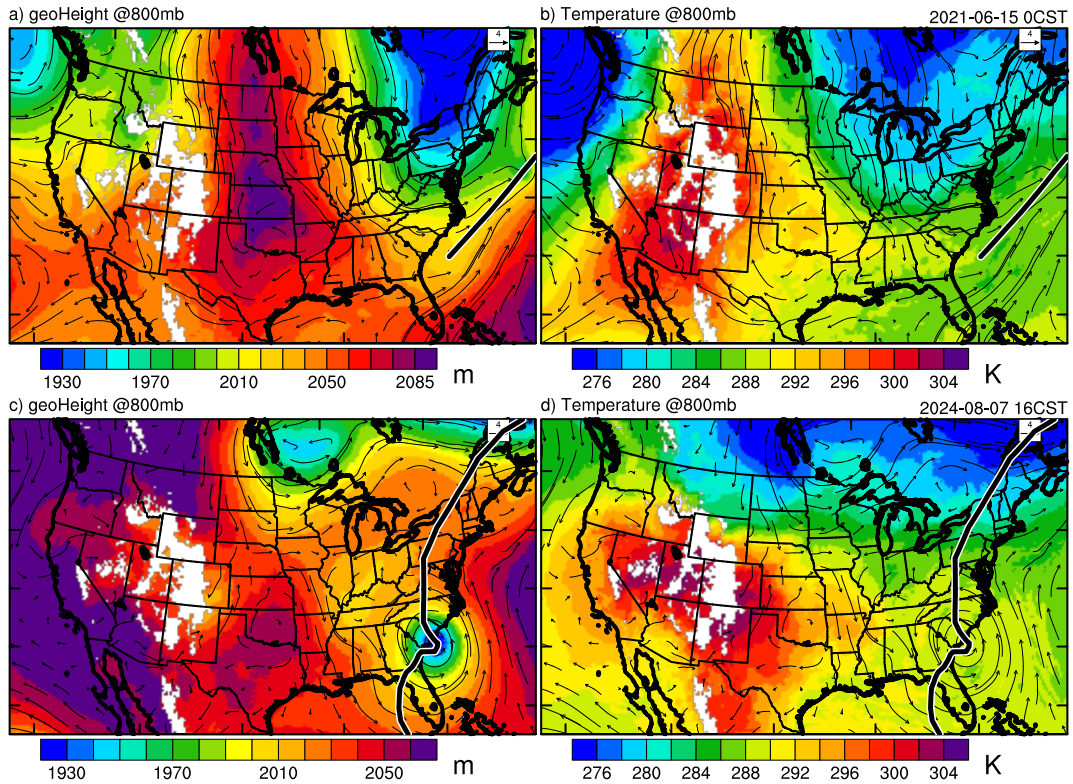


Figure 3. (a, c) Geopotential height and (b, d) temperature at 800 hPa on (top) 15 June 2021 and (bottom) 7 August 2024 simulated by WRF-Chem. Wind vectors are overlaid. Tracks of tropical cyclones Bill (2021) and Debby (2024) over the Atlantic Ocean are marked on top and bottom panels respectively.

automated meteorological stations, which expanded to 146 in 2025, and is designed to minimize the influence of urban landscapes (Basara et al., 2008; McPherson et al., 2007). Each Mesonet station measures more than 20 environmental variables, including wind speed and direction at 10 m and air temperature at 1.5 m above ground level (AGL). Oklahoma Mesonet data have been extensively used for weather forecasting and atmospheric research across the region (e.g., Hu, Klein, Xue, Lundquist, et al., 2013; Hu et al., 2016, 2023).

2.3. Design of WRF-Chem Simulations

WRF-Chem (version 4.6.1) simulations are conducted to examine the compound heat and O_3 pollution episode on 15 June 2021. The simulations are initialized at 0000 UTC on June 13 and run for 4 days. Our analyses focus on the later 3 days and exclude the first day when the model goes through spin-up. The initial and boundary conditions for meteorology are from hourly NCEP FNL (Final) operational global analysis and forecast (GFS) data at $0.25° \times 0.25°$ resolution (National Centers for Environmental Prediction, 2015) and those for chemistry are from the Whole Atmosphere Community Climate Model (WACCM) outputs with a resolution of $0.9° \times 1.25°$ (Gettelman et al., 2019). Three one-way nested domains are run simultaneously with 12-, 4-km, and 800-m horizontal grid spacings covering the conterminous U.S., the SGP, and part of Oklahoma (including OKC and Tulsa), respectively (Figure 1). The configuration of the outer two domains is inherited from our earlier O_3 study over the SGP (Hu et al., 2019). To better resolve near-source emissions and fine-scale physical and chemical processes over Oklahoma, a third sub-kilometer resolution modeling domain is introduced.

All domains use 48 vertical levels extending from the surface to 100 hPa. The sigma levels and mid-layer heights of the lowest 20 model layers are shown in Table 1. Most of the physical parameterizations follow Hu et al. (2019), including the revised MM5 Monin-Obukhov surface layer scheme (Jiménez et al., 2012), the Dudhia shortwave radiation algorithm (Dudhia, 1989), and the rapid radiative transfer model (RRTM) (Mlawer et al., 1997) for longwave radiation. To simulate the bulk effects of urban areas on the atmosphere, the Noah land surface model (Chen & Dudhia, 2001) was adopted following the approach of Liu et al. (2006), which has been

21698996, 2026, 17, Downloaded from https://agupubs.onlinelibrary.wiley.com/doi/10.1029/2026JD046327 by University Of Oklahoma, Wiley Online Library on [12/10/2026]. See the Terms and Conditions (https://onlinelibrary.wiley.com/terms-and-conditions) on Wiley Online Library for rules of use; OA articles are governed by the applicable Creative Commons License

21698996, 2026, 17, Downloaded from https://agupubs.onlinelibrary.wiley.com/doi/10.1029/2026JD046327 by University Of Oklahoma, Wiley Online Library on [12/10/2026]. See the Terms and Conditions (https://onlinelibrary.wiley.com/terms-and-conditions) on Wiley Online Library for rules of use; OA articles are governed by the applicable Creative Commons License

Table 1
Sigma Levels and Mid-Layer Heights (m AGL) of the Lowest 20 Model Layers

Sigma levels	1.0	0.997	0.994	0.991	0.988	0.985	0.975	0.97	0.96	0.95
Mid-layer heights	12	37	61	86	111	144	186	227	290	374
Sigma levels	0.94	0.93	0.92	0.91	0.895	0.88	0.865	0.85	0.825	0.8
Mid-layer heights	459	545	631	717	826	958	1,092	1,226	1,409	1,640

successfully applied to the same region. This simplified land-surface treatment appears to capture the first-order urban effects in the OKC metropolitan area reasonably well (Liu et al., 2006). Since the study period was free of clouds and precipitation over Oklahoma, microphysics and cumulus schemes are not expected to play a major role in the simulation results.

Since a grid spacing of 800 m is within the gray zone resolution, the scale-aware nonlocal Shin-Hong planetary boundary layer (PBL) scheme (Shin & Hong, 2015) is chosen for turbulent mixing. This scheme adopts a nonlocal heat flux profile fitted to Large-Eddy Simulation (LES) results and achieves scale-awareness (or horizontal grid spacing dependency) through scaling both local and nonlocal eddy fluxes according to the normalized grid spacing.

The gas-phase chemical reactions are simulated using the Regional Atmospheric Chemistry Mechanism (RACM, Stockwell et al., 1997), which is implemented within WRF-Chem using the Kinetic Preprocessor (KPP, Sandu et al., 2003). Biogenic emissions are calculated using the Model of Emissions of Gas and Aerosols from Nature (MEGAN) (Guenther et al., 2006). Abundant biogenic VOC emissions are generated over eastern Oklahoma and surrounding regions, where forest coverage, leaf area index, and vegetation fraction are high during summer (Wang et al., 2024). Consequently, O_3 formation in the downstream region becomes NOx-limited. The anthropogenic emission data are processed using the 1-km Neighborhood Emission Mapping Operation (NEMO, Ma & Tong, 2022). This data set is produced hourly based on the U.S. Environmental Protection Agency (EPA) 2019 National Emission Inventories (NEIs) Collaborative. There are hundreds of individual emission sources in the 2019 NEI, which are grouped into 16 emission sectors, including eight nonpoint sectors, two mobile sectors (on-road and off-road), and six point sectors (including EGUs, oil and gas production, and airports) (EPA, 2025; Ma & Tong, 2022). The spatial allocation was conducted by distributing county-level emission sources to model grids.

To further examine the contribution of anthropogenic NO_x emissions from power plants and Tulsa urban area on O_3 pollution in OKC, a set of WRF-Chem source sensitivity simulations (summarized in Table 2) are conducted using the brute force method, in which one specific source is modulated and the differences between the results from the sensitivity and baseline simulations are attributed to the modulated source (Cohan et al., 2005; Kiesewetter et al., 2015; Van Dingenen et al., 2018). In the CutElevated experiment, elevated NO_x emissions associated primarily with EGU power plants near Tulsa are removed to isolate their impact. In the CutSurfEle experiment, both aggregated surface and elevated NO_x emissions from Tulsa are removed to assess the combined impact of urban and power plant sources.

Table 2
Model Configuration for WRF-Chem Sensitivity Simulations With Modified Emissions

Experiment name	Emissions
Control	Emission data are processed using the Neighborhood Emission Mapping Operation (NEMO, Ma & Tong, 2022). This data set is produced hourly based on the United States Environmental Protection Agency (US EPA) National Emission Inventory 2019. The spatial allocation was conducted by distributing county-level emission sources to model grid
CutElevated	The elevated NOx emissions dominated by power plants over the Tulsa metropolitan area are removed
CutSurfEle	Both surface and elevated NOx emissions over the Tulsa metropolitan area are removed (see the emission mask in Figure 8b)

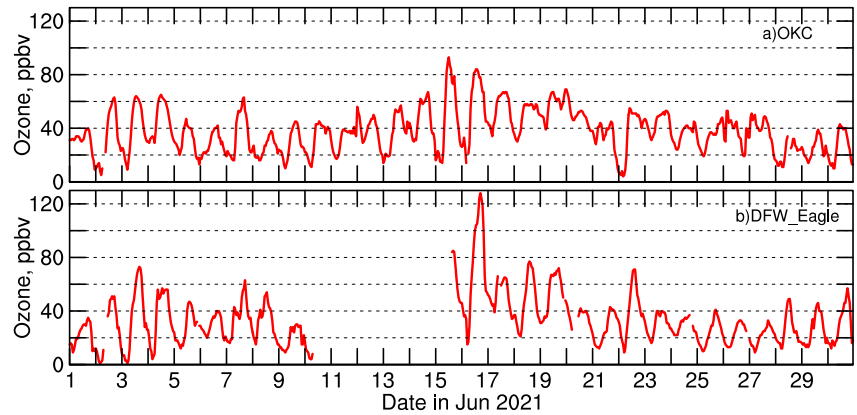


Figure 4. Time series of hourly O_3 during June 2021 at (a) OKC and (b) Eagle in the Dallas-Fort Worth (DFW) area.

3. Results

3.1. Synoptic and Mesoscale Meteorological Conditions

During 15–16 June 2021, a compound heat and O_3 pollution event occurred in the SGP. The heat wave was intensified by the combined effects of synoptic-scale circulation and local terrain influences. A persistent high-pressure center and its associated anticyclonic circulation dominated the SGP during this period (Figures 2 and 3a), providing favorable large-scale dynamical conditions for subsidence. In addition, during summer, the Rocky Mountains to the west of the SGP act as elevated heat sources due to strong absorption of solar radiation (Ye, 1981), resulting in temperatures warmer than the surrounding air at the same altitude (Figure 3b). This thermal contrast induces a mountain–plains solenoid circulation (Bao et al., 2011; Hu et al., 2014; Qian et al., 2015), characterized by rising motion over the mountains and sinking motion over the SGP to the east. The downward branch of this thermally driven circulation over the SGP reinforces large-scale subsidence and further intensifies the heat wave. Enhanced subsidence strengthens the capping inversion over the boundary layer, thereby suppressing vertical mixing and exacerbating air pollution, a mechanism comparable to that frequently documented over the North China Plain east of the Loess Plateau (Hu et al., 2014).

In addition, the O_3 pollution observed in OKC (with a maximum of 93 ppbv on 15 June) and in DFW (maximum of 128 ppbv on 16 June) (Figure 4) coincided with the passage of a cold frontal system over the SGP, which was dynamically linked to the development of the tropical storm Bill off the eastern U.S. coast (Figure 2b). The storm started as a tropical depression east of South Carolina on 14 June and intensified into a tropical storm on 15 June and moved straight to northeast direction. On 15 June, the associated cold front approached the northeast corner of Oklahoma (Figure 2b). Wind speed over the area ahead of the cold front including the OKC metropolitan area was weak as observed by the Oklahoma Mesonet sites (Figure 5). On the same day, the peak hourly O_3 level observed in OKC represented the second-highest hourly O_3 mixing ratio recorded during 2014–2022, following the highest O_3 level of 106 ppbv on 19 July 2018. On 16 June, the cold front weakened and transitioned to a stationary front that persisted near the eastern border of Oklahoma and Texas (Figure 2c). During this period, widespread O_3 pollution developed in the DFW area with hourly O_3 concentrations well above 100 ppbv (Figure 4).

The synoptic evolution of this episode closely resembles the two severe O_3 pollution events over DFW reported by Hu et al. (2019), which were linked to the passage of Atlantic hurricanes along the U.S. east coast. This case thus further confirms the conclusion of Hu et al. (2019) that the dead-wind or convergence zones ahead of hurricane- or tropical cyclone-associated fronts can lead to O_3-precursor accumulation and rapid O_3 formation over urban areas in the SGP. This study finds that this O_3 formation mechanism contributes to O_3 pollution not only in the DFW area but also in OKC. Consistent behavior is also evident in the 19 July 2018 case, characterized by weak winds and poor dispersion within the convergence zone ahead of a cold front (Figure not shown). These events indicate that severe O_3 pollution in the SGP is unlikely under typical summertime conditions dominated by strong southerly flow on the western flank of the Bermuda High, which generally favors effective ventilation (Sumner, 2025; Zhu & Liang, 2013). In contrast, extreme O_3 pollution in the region tends to develop only in the

21698996, 2026, 17, Downloaded from https://agupubs.onlinelibrary.wiley.com/doi/10.1029/2026JD046327 by University Of Oklahoma, Wiley Online Library on [12/10/2026]. See the Terms and Conditions (https://onlinelibrary.wiley.com/terms-and-conditions) on Wiley Online Library for rules of use; OA articles are governed by the applicable Creative Commons License

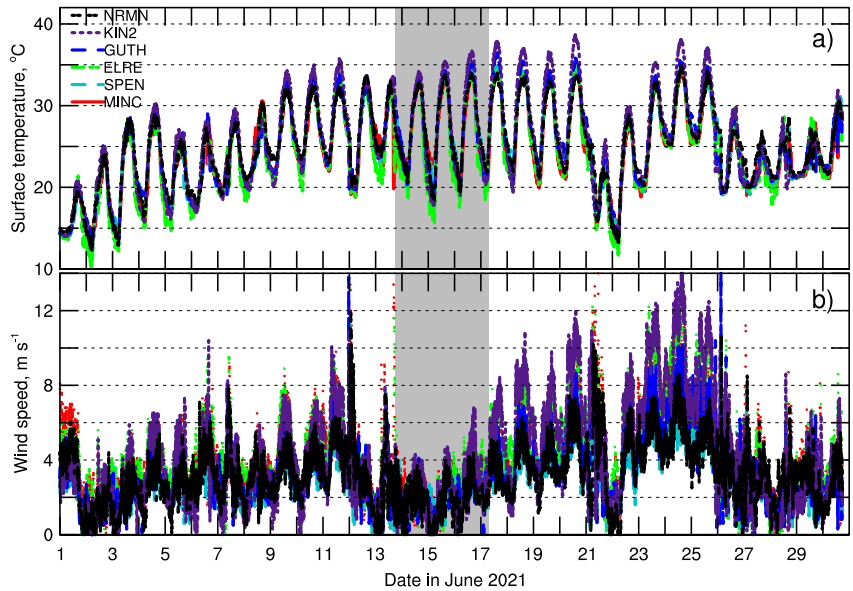


Figure 5. Time series of (a) surface temperature and (b) wind speed at the six Mesonet sites surrounding the OKC metropolitan area (i.e., El Reno (ELRE), Guthrie (GUTH), Kingfisher (KIN2), Minco (MINC), Norman (NRMN), and Spencer (SPEN)) during June 2021. The selected episode is shaded in gray.

presence of specific transient conditions, particularly frontal passages that generate stagnant prefrontal environments.

3.2. Regional Emission Sources and Transport Toward Oklahoma City

In addition to mesoscale meteorological conditions, unique regional emission drivers also contributed to the event observed in OKC on 15 June 2021. On the preceding day (June 14), a weak high-pressure system was centered over Kansas (Figure 2a), with northeasterly winds prevailing across eastern Oklahoma (Figure 6). WRF-Chem simulations clearly show four distinct SO_2 plumes emitted from major electricity-generating power plants within the model domain. Three of them originated from facilities surrounding Tulsa, namely the Muskogee, Grand River, and Northeastern power plants (Figure 1b). These facilities are fueled by natural gas and coal. Since coal combustion is a dominant source of SO_2 (de Gouw et al., 2014), these emissions produce clearly identifiable SO_2 plumes that can serve as tracers for power plant outflows.

NO_x, key precursors of O_3 formation, were co-emitted from these power plants and the Tulsa metropolitan area (as observed by TROPOMI, Figure 7). Notably, TROPOMI observations of column-integrated NO_2 (XNO_2) show that power plants and urban areas are the dominant sources of NO_x in the region (Figure 7), indicating their major contribution to O_3 pollution in Oklahoma. Both satellite observations and WRF-Chem simulations show southwestward transport of these NO_x-rich plumes toward central Oklahoma (Figure 7a). On 15 June as the cold front approached the northeastern corner of Oklahoma, a weak high-pressure system was centered over the state (Figures 2b and 3a), resulting in weak winds over the OKC area (Figure 6). Under these conditions, pollutant plumes from the Tulsa metropolitan area continued to be transported toward OKC, where they accumulated and contributed to elevated O_3 concentrations. Note that, modeled XNO_2 exhibits a positive bias of $\sim$1–2 $\times$ 10^{15} molecules cm^{-2} at the urban maximum over OKC relative to TROPOMI on both 14 and 15 June, while a negative bias is evident over the surrounding wide rural areas on 15 June. This urban–rural contrast in XNO_2 bias is consistent with that reported in WRF–CMAQ simulations over the continental United States during summer 2020 (Ma et al., 2025).

21698996, 2026, 17, Downloaded from https://agupubs.onlinelibrary.wiley.com/doi/10.1029/2026JD046327 by University Of Oklahoma, Wiley Online Library on [12/10/2026]. See the Terms and Conditions (https://onlinelibrary.wiley.com/terms-and-conditions) on Wiley Online Library for rules of use; OA articles are governed by the applicable Creative Commons License

21698996, 2026, 17, Downloaded from https://agupubs.onlinelibrary.wiley.com/doi/10.1029/2026JD046327 by University Of Oklahoma, Wiley Online Library on [12/10/2026]. See the Terms and Conditions (https://onlinelibrary.wiley.com/terms-and-conditions) on Wiley Online Library for rules of use; OA articles are governed by the applicable Creative Commons License

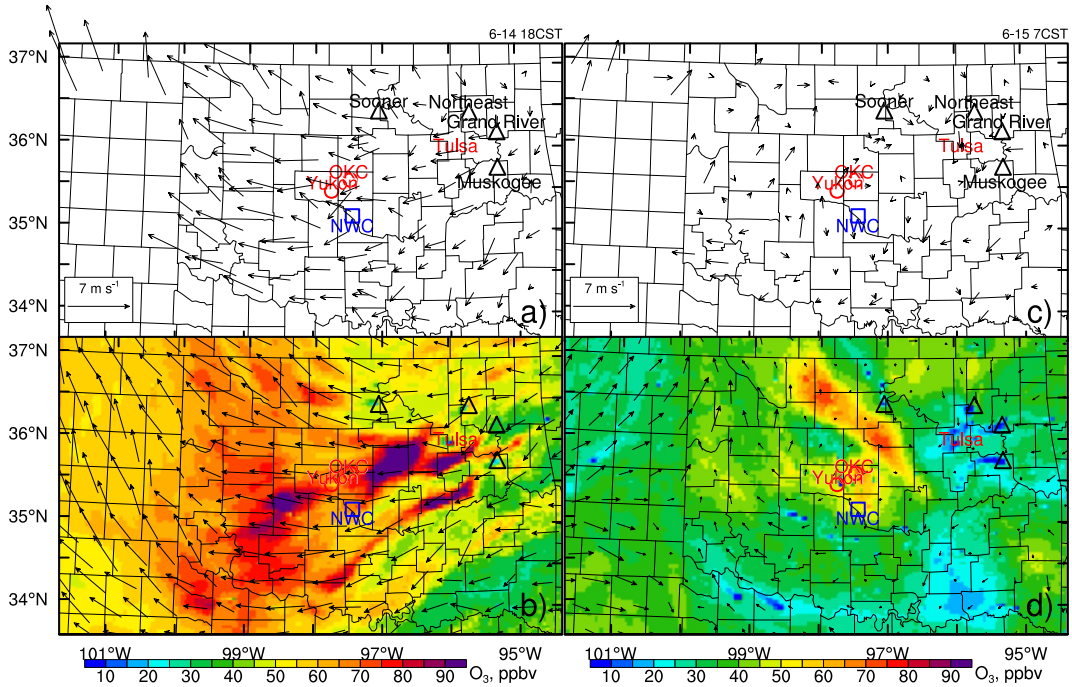


Figure 6. Wind fields (a, c) observed over Oklahoma Mesonet sites and (b, d) simulated with WRF-Chem at (left) 18 CST on 14 June and (right) 7 CST on 15 June 2021. Simulated O_3 plumes are also overlaid in panels (b, d).

3.3. Model Quantification of Impact of Emission and Meteorology Drivers

3.3.1. Model Evaluation in Terms of Reproducing the Compound Event

To further examine these processes and quantify the contribution of emissions from power plants and Tulsa urban area to O_3 pollution in OKC, WRF-Chem simulations with default emissions and with NOx emissions removed

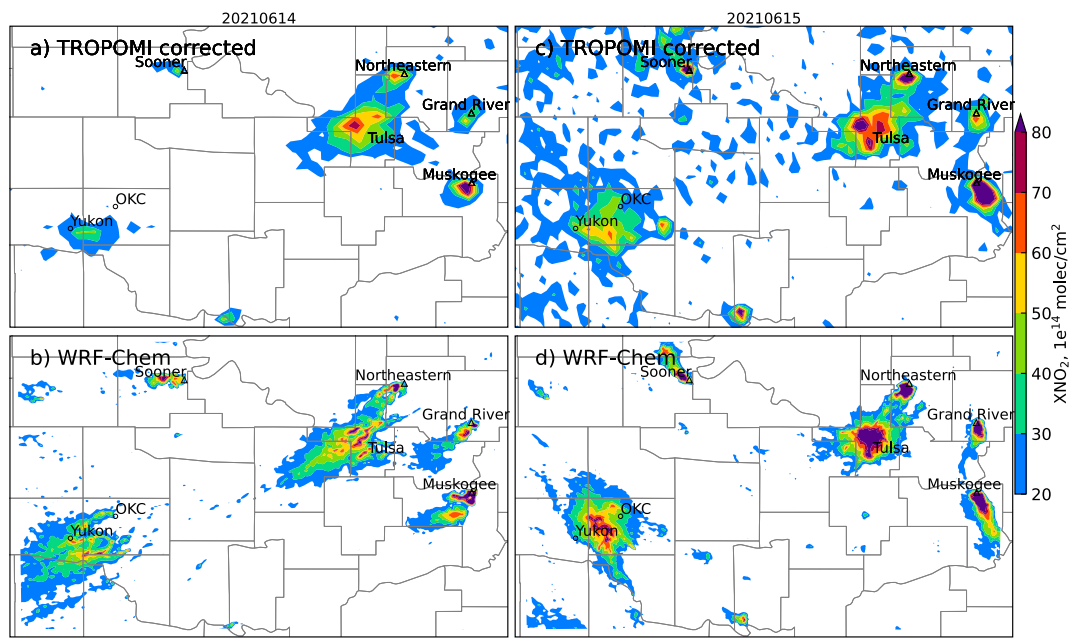


Figure 7. Column NO_2 (a, c) observed by TROPOMI and (b, d) simulated with WRF-Chem on (left) 14 and (right) 15 June 2021. Note that TROPOMI XNO_2 is corrected using the air mass factor (AMF) calculated using NO_2 profiles simulated with WRF-Chem following Equations 1–3.

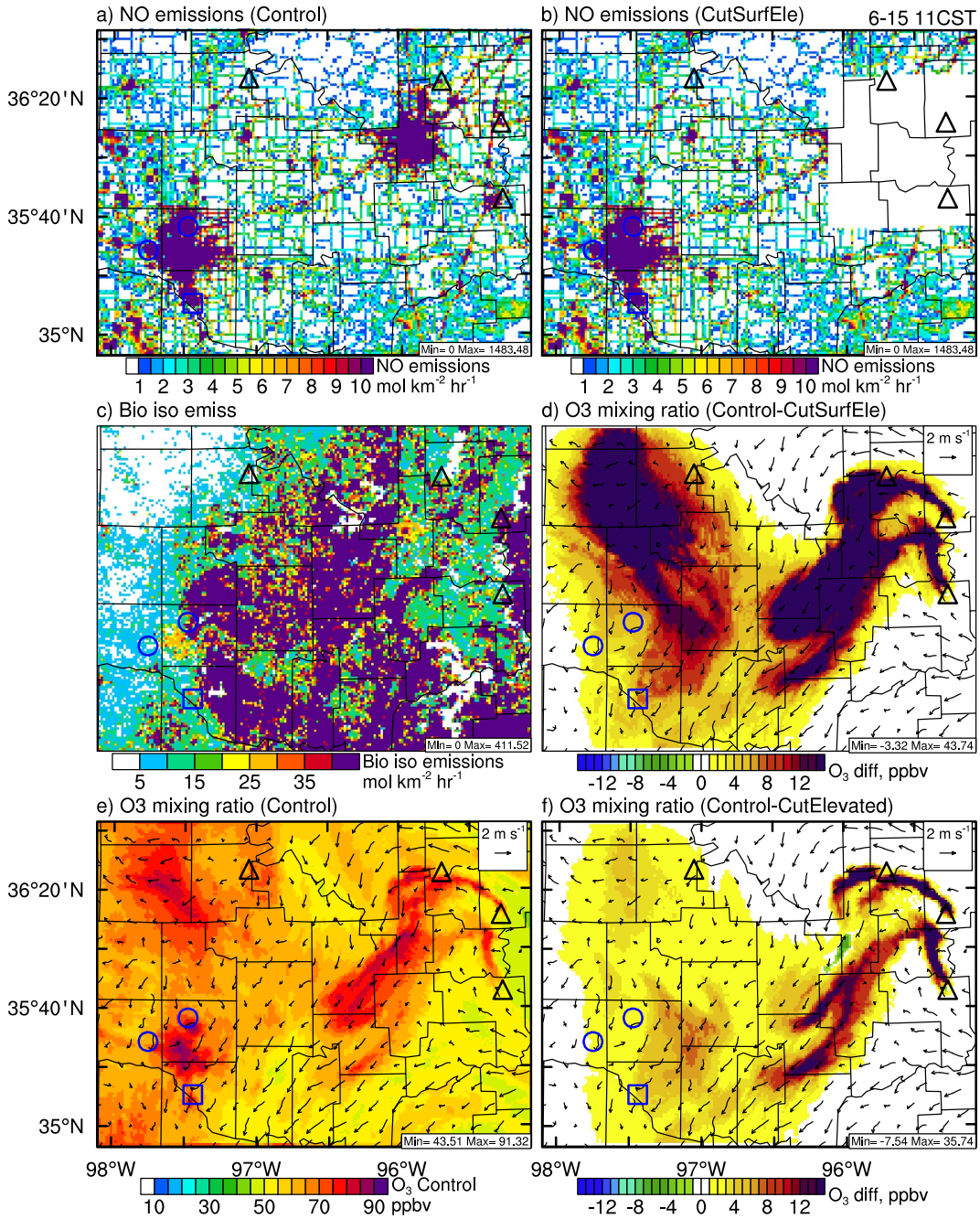


Figure 8. NO emissions used by WRF-Chem (a) Control and (b) CutSurfEle sensitivity simulation, and (c) Biogenic isoprene emissions, (e) O_3 simulated by the control, (d) O_3 difference between Control and CutSurfEle simulations and (f) O_3 difference between Control and CutElevated simulations at 11 CST on 15 June 2021.

over the Tulsa area are conducted (Figure 8). The large biogenic VOC emissions over eastern Oklahoma (Figure 8c) shift downstream O_3 formation into a NOx-limited regime. Therefore, the brute-force sensitivity simulations focus on NOx emissions. The control WRF-Chem simulation with default emissions is evaluated against surface meteorological, satellite, and O_3 observations. The model reproduces the variation of temperature and winds recorded by Oklahoma Mesonet stations (Table 3) and captures the multi-day heat wave over Oklahoma quite well, with a slight underestimation of near-surface air temperature at sunrise time (~1.5°C). The overall mean temperature bias is −0.18°C, corresponding to a normalized mean bias of −0.7%. Particularly, the model captures the increasing trend of the daily temperature maximum during this episode, suggesting that the

21698996, 2026, 17, Downloaded from https://agupubs.onlinelibrary.wiley.com/doi/10.1029/2026JD046327 by University Of Oklahoma, Wiley Online Library on [12/10/2026]. See the Terms and Conditions (https://onlinelibrary.wiley.com/terms-and-conditions) on Wiley Online Library for rules of use; OA articles are governed by the applicable Creative Commons License

21698996, 2026, 17, Downloaded from https://agupubs.onlinelibrary.wiley.com/doi/10.1029/2026JD046327 by University Of Oklahoma, Wiley Online Library on [12/10/2026]. See the Terms and Conditions (https://onlinelibrary.wiley.com/terms-and-conditions) on Wiley Online Library for rules of use; OA articles are governed by the applicable Creative Commons License

Table 3
Evaluation Statistics for Simulated Hourly 2-m Temperature (T_2) and 10-m Wind Speed Against the Oklahoma Mesonet Data During 13–16 June 2021

	T_2 (°C)	10-m wind speed (m s^{-1})
Mean observation	27.0	2.2
Number of data	11,433	11,433
Mean simulation	26.8	2.4
MB	−0.18	0.27
RMSE	1.9	1.3
NMB	−0.7%	12.5%
Correlation coefficient	0.94	0.59

Note. The metrics include mean bias (MB), root mean-square error (RMSE), normalized mean bias (NMB), and correlation coefficient. Their formulas can be found in Yu et al. (2006). These statistical metrics are commonly used in numerical air quality model evaluations (e.g., Hu, Klein, & Xue, 2013; Hu et al., 2010, 2019, 2021).

simulation reasonably represents the background thermal conditions relevant for O_3 formation (Figure 9). The model overestimates surface wind speed by 0.27 m s^{-1} (Table 3), particularly during nighttime (Figure 9), presumably in part because the influence of obstructions and roughness on the surface winds is generally underestimated (Fovell & Gallagher, 2020; Hu et al., 2023; Shen et al., 2022).

The ability of WRF-Chem to reproduce observed O_3 variability is evaluated using hourly surface O_3 measurements at the OKC and Yukon EPA monitoring sites (Figure 10). The model captures the day-to-day variation and timing of daytime maximum O_3 during 14–16 June 2021, including the second-highest O_3 pollution episode recorded during 2014–2022 at both sites. WRF-Chem also captures the decrease in surface O_3 on 16 June associated with the shift to stronger southerly winds and improved ventilation over the OKC metropolitan area (Figure 5). Larger discrepancies are evident on 13 June, when the model is still influenced by spin-up effects.

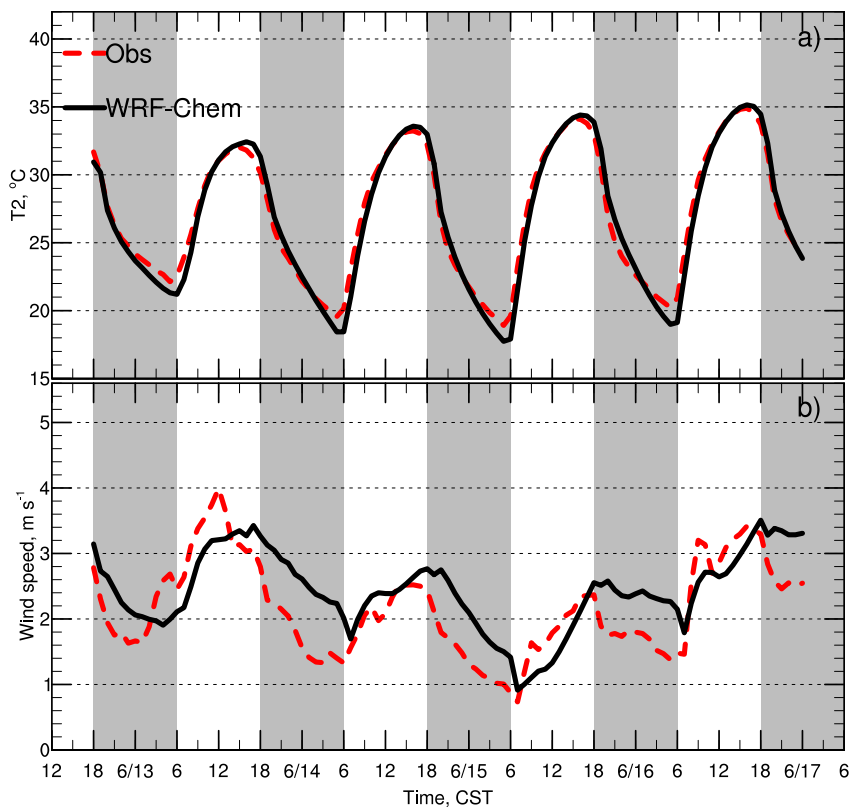


Figure 9. Average (a) 2-m temperature (T2) and (b) 10-m wind speed during 13–16 June 2021 observed at 110 Oklahoma Mesonet sites and simulated with WRF-Chem. Nighttime is shaded in gray.

21698996, 2026, 17, Downloaded from https://agupubs.onlinelibrary.wiley.com/doi/10.1029/2026JD046327 by University Of Oklahoma, Wiley Online Library on [12/10/2026]. See the Terms and Conditions (https://onlinelibrary.wiley.com/terms-and-conditions) on Wiley Online Library for rules of use; OA articles are governed by the applicable Creative Commons License

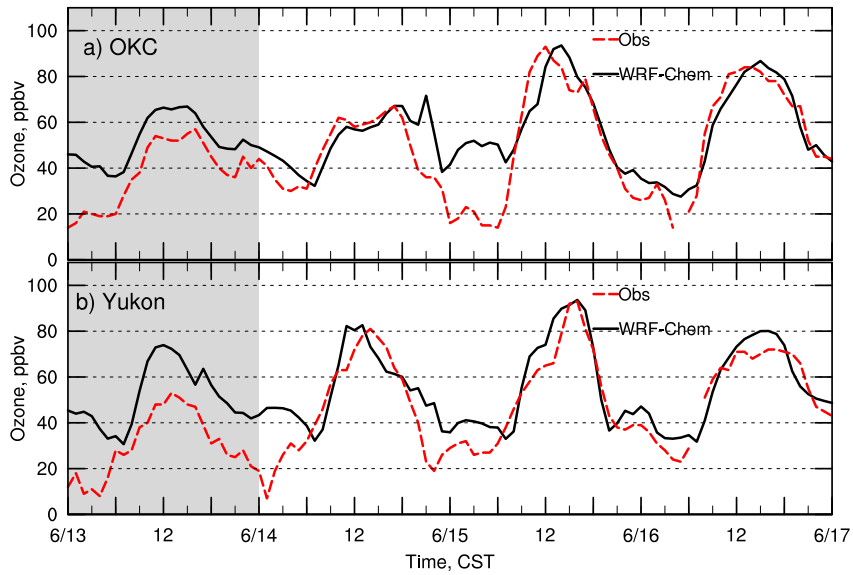


Figure 10. Hourly O_3 during 13–16 June 2021 observed and simulated with WRF-Chem at (a) the OKC and (b) Yukon EPA monitoring sites (see their locations in Figure 1b). Model spin-up period is shaded in gray.

Meanwhile, the model also exhibits larger positive O_3 biases during nighttime than during daytime. Such nighttime overestimation is a long-standing challenge in air quality modeling (Huang et al., 2025) and may be attributable to biases in nighttime surface emissions and/or excessive vertical mixing, which is commonly found in operational numerical weather prediction and climate models (Bechtold et al., 2008; Hu et al., 2010; Louis, 1979; McNider et al., 2018). The frequent occurrence of nocturnal LLJs over the SGP (Klein et al., 2014, 2015) further complicates nighttime O_3 behavior and poses additional challenges for model representation in this region (Hu, 2015; Hu, Klein, & Xue, 2013).

The model's representation of O_3 precursor distributions is further evaluated using satellite observations of XNO_2. Figure 7 compares corrected TROPOMI XNO_2 with WRF-Chem simulations on 14 and 15 June 2021. TROPOMI observations reveal pronounced NO_2 enhancements over major emission sources in northeastern Oklahoma, including the Tulsa metropolitan area and nearby power plants (Muskogee, Grand River, and Northeastern), with plume orientations indicating southwestward transport toward OKC at the satellite overpassing time on 14 June. WRF-Chem reproduces the primary spatial features observed by TROPOMI, including XNO_2 hotspots over urban areas and point sources and the regional transport pathways toward the OKC metropolitan area. Although the bias in model-satellite comparison of XNO_2 plumes can be noticed (likely due to different vertical and horizontal resolutions used by satellite retrieval and model simulation), the model captures the magnitude and structure of distributions, providing confidence in its representation of emissions and transport and their impact on O_3 pollution during this event.

3.3.2. Contributions of Tulsa NO_x Emissions on O_3 Pollution Over OKC

Differences between the control and sensitivity WRF-Chem simulations illustrate the impact of NO_x emissions from Tulsa and surrounding areas on the O_3 pollution across the domain. The O_3 difference between the control and CutSurfEle runs (Figure 8d) shows a southwestward-extending O_3 plume originating from the Tulsa area and enhancing O_3 levels over OKC. Depending on location, O_3 differences reached up to ~30 ppbv within the domain (Figure 8d). The O_3 enhancement over OKC on 15 June can be traced back to O_3 plumes generated from Tulsa area on both 14 and 15 June (Figures 11a–11c). Cross-sections along the OKC–Tulsa transect (Figures 11a–11c) show that the O_3 plume downwind of Tulsa is gradually transported toward OKC and resides in the residual layer above the stable boundary layer on the night of 14–15 June. The O_3 mixing ratio exceeded 100 ppbv in this aged residual layer plume over OKC (Figure 11c). Process analysis further confirms the positive contribution of advection at 21 CST on the night. At this time, advection of O_3 exceeds 10 ppbv hr^{-1} at 400–500 m above ground within the residual layer, whereas chemical reactions (dominated by nitric oxide (NO) titration) remove near-surface O_3, and vertical mixing acts to replenish surface O_3 (Figure 12a). As the daytime convective boundary

21698996, 2026, 17, Downloaded from https://agupubs.onlinelibrary.wiley.com/doi/10.1029/2026JD046327 by University Of Oklahoma, Wiley Online Library on [12/10/2026]. See the Terms and Conditions (https://onlinelibrary.wiley.com/terms-and-conditions) on Wiley Online Library for rules of use; OA articles are governed by the applicable Creative Commons License

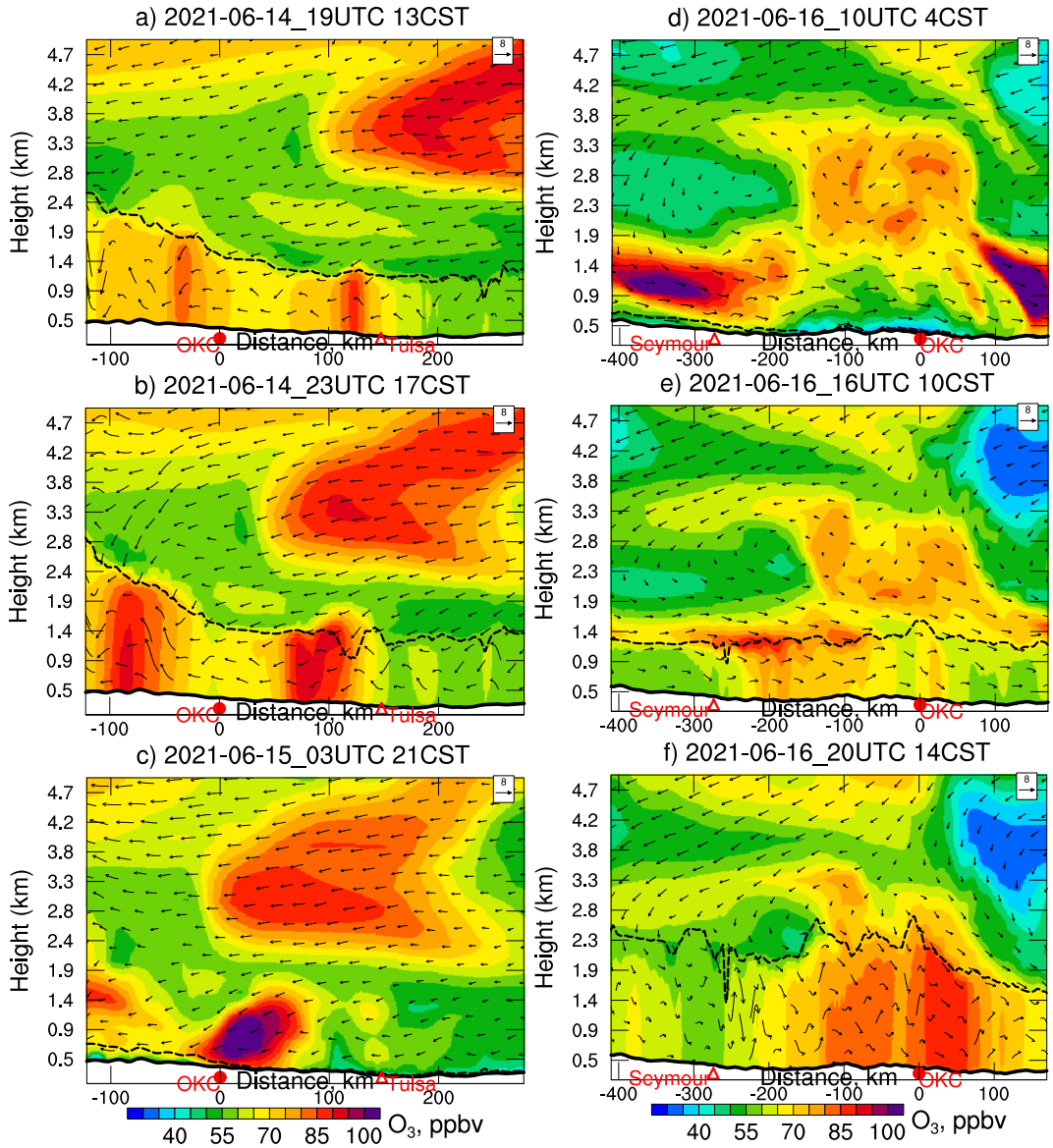


Figure 11. Cross-sections of O_3 and winds during 14–16 June 2021 along transects inclined (a–c) 70° and (d–f) 35° from the south–north direction: the left transect passes through OKC and Tulsa, while the right transect passes through OKC and Seymour, Texas. The boundary layer top is marked by dashed lines.

layer develops, this O_3-rich residual-layer air is entrained into the mixed layer, contributing to the rapid morning increase in boundary-layer O_3 on 15 June. This boundary-layer O_3 formation mechanism has been documented previously (Hu, Klein, Xue, Zhang, et al., 2013; Morris et al., 2010; Zhang & Rao, 1999). At midday, chemical production dominates (>10 ppbv hr^{-1}) boundary-layer O_3, exceeding advection and vertical mixing (Figure 12b). It enhances O_3 in the mid-boundary layer due to net production of NO_x–VOC photochemistry but depletes O_3 near the surface due to rapid NO titration (Hu et al., 2012, 2019; Sillman, 1999). The resulting O_3 is redistributed by vertical mixing, increasing surface concentrations but reducing levels in the mid-boundary layer (Figure 12b).

On 15 June, O_3 enhancements attributed to Tulsa emissions varied between 6 and 15 ppbv at the OKC site and 4–10 ppbv at the Yukon site (Figure 13), suggesting the combined influence of regional transport and favorable local photochemical production. In comparison, larger O_3 enhancement of 20–40 ppbv appeared near the northwest corner of the innermost domain but did not lead to severe surface O_3 pollution, mainly because local O_3 formation is weak in regions with low anthropogenic emission density. Although OKC did not experience the

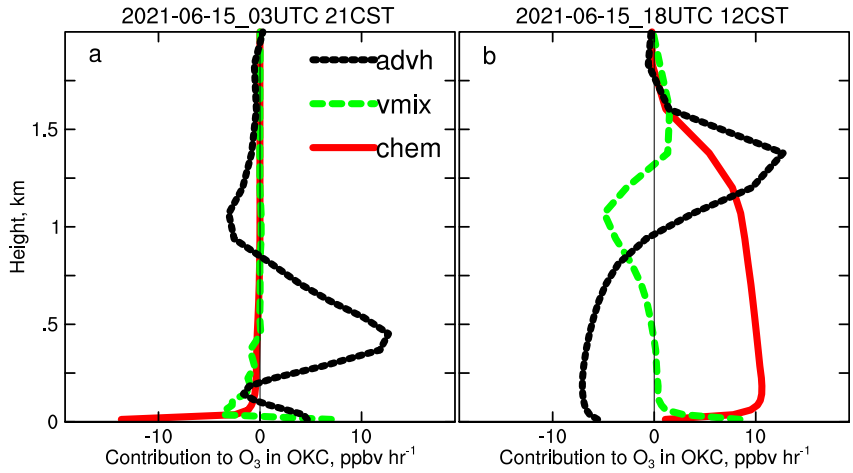


Figure 12. Contribution to O_3 accumulation over OKC by different processes, including horizontal advection (advh), vertical mixing (vmix), and chemical reactions (chem) at (a) 0300 and (b) 1800 UTC on 15 June 2021.

highest O_3 enhancement originating from Tulsa (Figure 8), severe O_3 pollution occurred over OKC because regional transport was superimposed on the prominent local O_3 formation. The contribution of Tulsa plumes to O_3 in the OKC metropolitan area on other days was relatively minor (Figure 13). These results confirm that the Tulsa plumes indeed played a substantial role in producing the O_3 pollution episode observed in OKC on 15 June, which was the second-worst during 2014–2022.

The impact of elevated sources in Tulsa (Control minus CutElevated) is shown in Figure 8f. Although all elevated emissions within the Tulsa area were removed in CutElevated (Figure 8b), the resulting response is dominated by plumes associated with the three major power plants in the region (Figure 8f), indicating that these facilities account for most elevated emissions in the masked area. The CutElevated sensitivity simulation indicates that power plants alone contributed ~2–6 ppbv of O_3 to the OKC metropolitan area on 15 June, depending on time and location (Figure 13). These results confirm that under favorable conditions, power plant emissions from the Tulsa metropolitan area could cause O_3 exceedance in OKC. The impacts of Tulsa emissions on O_3 pollution in OKC were not limited to the surface but extended throughout the whole boundary layer (Figure 14). Some of the

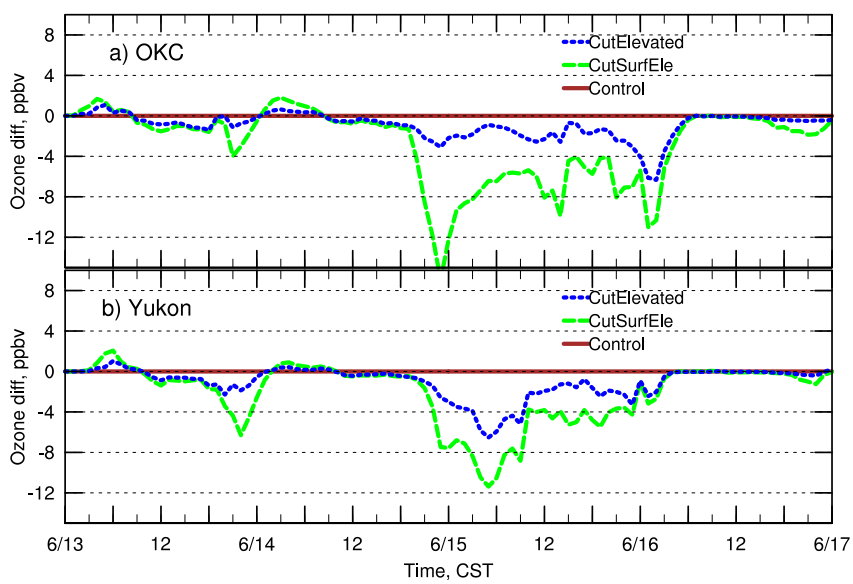


Figure 13. Simulated differences in hourly O_3 concentrations during 13–16 June 2021 between the control and sensitivity WRF-Chem simulations at (a) the OKC and (b) Yukon EPA monitoring sites.

21698996, 2026, 17, Downloaded from https://agupubs.onlinelibrary.wiley.com/doi/10.1029/2026JD046327 by University Of Oklahoma, Wiley Online Library on [12/10/2026]. See the Terms and Conditions (https://onlinelibrary.wiley.com/terms-and-conditions) on Wiley Online Library for rules of use; OA articles are governed by the applicable Creative Commons License

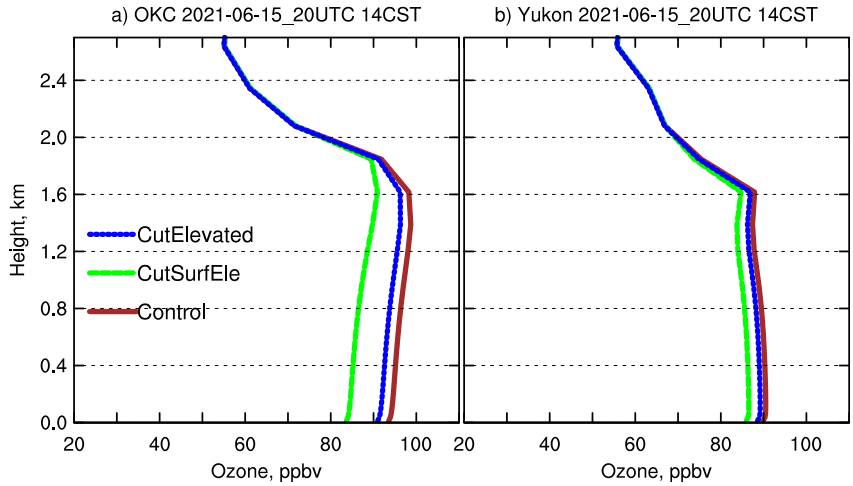


Figure 14. Simulated differences in vertical O_3 profiles between the control and sensitivity WRF-Chem simulations at (a) the OKC and (b) Yukon EPA monitoring sites at 14 CST, 15 June 2021.

pollutant plumes were transported southwestward within the shallower boundary layer during the nighttime of 14–15 June, which were subsequently well mixed into the growing convective boundary layer on 15 June.

3.3.3. Event Evolution on 16 June and Boundary Layer Structure

On 16 June, southerly winds dominated over the OKC area. In the absence of southwestward transport from the Tulsa region, surface O_3 levels over OKC decreased (Figure 10). Regional transport from DFW instead appears to have contributed modestly to O_3 levels over OKC on this day (Figures 11d–11f). On 15 June, an O_3 plume from DFW is transported westward to Seymour and resides in the residual layer above the stable boundary layer overnight (Figure 11d). Subsequently, as the prevailing winds shift to southwesterly, the plume is advected toward OKC. On the next morning, entrainment at the top of the convective boundary layer mixes the residual-layer O_3 into the boundary layer (Figure 11e), eventually contributing to daytime O_3 over OKC on 16 June (Figure 11f). However, the contribution from the DFW O_3 plume was insufficient to lead to severe O_3 pollution over OKC due to favorable dispersion conditions. This is consistent with previous studies showing that strong southerly prevailing winds generally inhibit severe O_3 buildup over OKC (Hu, Klein, & Xue, 2013; Zhu & Liang, 2013).

An ozonesonde launched at 1600 CST on 16 June from the National Weather Center (see its location in Figure 1b) showed an approximately 15 ppbv O_3 enhancement within the boundary layer. Because the National Weather Center is located near the southern edge of Oklahoma City, where local emissions are relatively weak, this observation further supports the conclusion that northward transport of pollutants from DFW contributed to this boundary layer O_3 enhancement. An overestimation of the boundary layer height by ~400 m at this time is evident from the comparison of the vertical O_3 profiles (Figure 15). This overestimation extends from the DFW region to the SGP ARM site in northern Oklahoma (Figures 16b and 16d) and can be traced back to similar biases in the driving FNL meteorological fields. The underlying causes of this bias, potentially related to land surface representation of FNL over the SGP, are beyond the scope of this study. Note that such overestimation is not evident earlier during the 14–16 June episode. For example, on the afternoon of 14 June, WRF-Chem captures the observed boundary layer structure from DFW to the SGP ARM site quite well (Figures 16a and 16c).

3.4. Additional Compound Heat and O_3 Pollution Episode Over Oklahoma Influenced by an Atlantic Tropical Cyclone

Compound heat and O_3 episodes in OKC coinciding with the passage of Atlantic tropical storms have also been identified in other cases, including Hurricane Debby on 6–7 August 2024 (Figures 3c and 3d). During this episode, hourly O_3 reached 86 ppbv and the maximum temperature reached 39°C at OKC, indicating a compound heat and O_3 pollution event (Figure 17). A stationary front influenced by Hurricane Debby persisted to the southwest of OKC. As a result, O_3 plumes from Tulsa area and the surrounding power plants are transported into the OKC metropolitan area (Figure 17a), exacerbating the compound heat and O_3 pollution hazard. Differences

21698996, 2026, 17, Downloaded from https://agupubs.onlinelibrary.wiley.com/doi/10.1029/2026JD046327 by University Of Oklahoma, Wiley Online Library on [12/10/2026]. See the Terms and Conditions (https://onlinelibrary.wiley.com/terms-and-conditions) on Wiley Online Library for rules of use; OA articles are governed by the applicable Creative Commons License

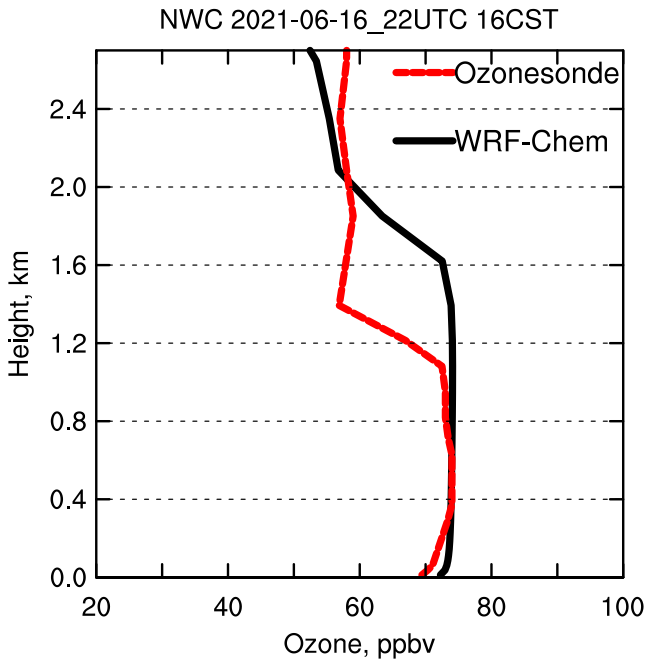


Figure 15. Vertical O_3 profiles at 1600 CST on 16 June 2021 observed and simulated by WRF-Chem at the National Weather Center in Norman, Oklahoma.

between the control and CutSurfEle simulations suggest that the Tulsa NO_x emissions contributed 6–24 ppbv daytime O_3 over OKC on 7–8 August 2024.

4. Conclusions and Discussion

Compound heat and O_3 pollution events have been widely observed and are often associated with significant environmental and public health impacts, particularly in regions experiencing intensifying heat extremes. In the SGP, where frequency and intensity of heat waves are projected to increase, understanding and modeling of these compound events is essential for improving risk assessment and informing mitigation strategies. This study investigates the three severe O_3 pollution episodes recorded in OKC since 2014, that is, 19 July 2018 (106 ppb), 15 June 2021 (93 ppb), and 6–7 August 2024 (86 ppb), with a primary focus on the 14–16 June 2021 episode, which coincided with a multi-day heat wave. TROPOMI satellite data indicate significant power plant emissions in addition to urban area emissions in the Tulsa region, which provide substantial precursors for O_3 formation in Oklahoma under favorable meteorology. Using high-resolution WRF-Chem simulations, we identify key meteorological and emission-related contributors. The June 2021 episode occurred under atypical summertime conditions over the SGP with frontal passage that was dynamically linked to the development of tropical cyclone Bill over the Atlantic Ocean. Ahead of the front, weak winds and a convergence zone formed over central Oklahoma, which substantially limited ventilation. Under these conditions, southwestward transport of pollutants from the Tulsa area (including both surface and elevated power plant emissions) on both 14 and 15 June provided additional O_3 precursors to OKC. The combination of sustained heat, clear skies, regional transport, and weak prefrontal winds promoted pollutant accumulation and efficient photochemical O_3 production, ultimately, leading to the severe O_3 pollution in OKC. Our study reinforces that severe O_3 exceedances in OKC are very rare under typical summer conditions dominated by strong southerly winds with effective dispersion, but can develop under specific transient meteorological conditions influenced by frontal passages.

WRF-Chem sensitivity simulations further quantify the contribution of regional emissions to the observed O_3 enhancements. On 15 June 2021, total NO_x emissions from the Tulsa area contribute ~4–15 ppbv of O_3 to OKC,

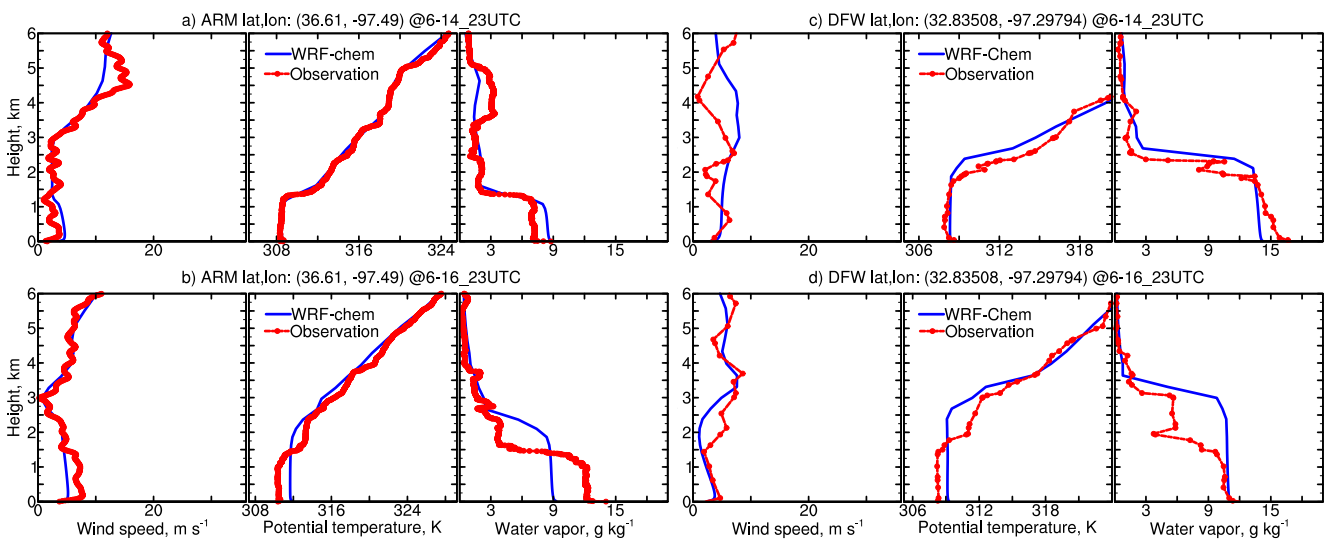


Figure 16. Observed and simulated profiles of (left to right) wind speed, potential temperature, and water vapor mixing ratios over (a, b) the SGP ARM site and (c, d) Dallas-Fort Worth at 1700 CST on (top) 14 and (bottom) 16 June 2021.

21698996, 2026, 17, Downloaded from https://agupubs.onlinelibrary.wiley.com/doi/10.1029/2026JD046327 by University Of Oklahoma, Wiley Online Library on [12/10/2026]. See the Terms and Conditions (https://onlinelibrary.wiley.com/terms-and-conditions) on Wiley Online Library for rules of use; OA articles are governed by the applicable Creative Commons License

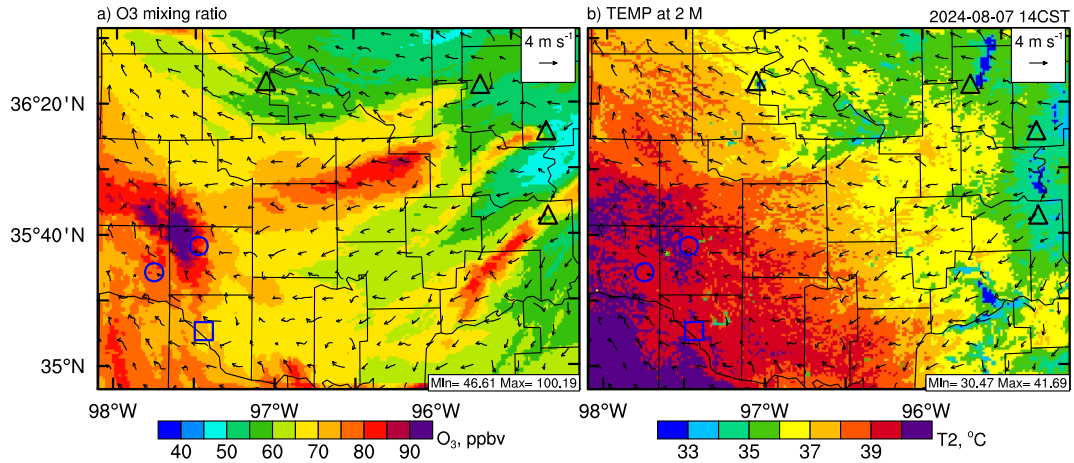


Figure 17. (a) O_3 and (b) 2-m temperature (T2) simulated by the control WRF-Chem simulation at 14 CST on 7 August 2024.

while power plants alone accounted for ∼2–6 ppbv depending on location and timing. Although power plants alone did not dominate O_3 production during the selected episode, their contribution was sufficient to promote O_3 exceedances under favorable meteorological conditions. Note that only the impact of NO_x emissions is examined in the sensitivity simulations; accounting for emissions of other precursors, such as CO, from these sources may result in a larger impact on regional O_3 levels. These results demonstrate that regional point sources can meaningfully influence urban O_3 levels when transport and stagnation coincide, even in cities located more than 100 km downwind.

The implications of these findings extend beyond the two events presented here. Power plants in the Tulsa area are fueled by coal or a combination of coal, gas, and oil and remain important regional NO_x sources. Recent U.S. policy developments emphasizing energy security and affordability, along with compliance extensions granted for some facilities, suggest that these sources are likely to remain active in the near future. Meanwhile, rapidly increasing electricity demand in the region, driven in part by the expansion of data centers and related facilities, may further increase emissions from these power plants during peak demand periods. Consequently, emissions from the Tulsa area may remain a significant contributor to O_3 pollution in central Oklahoma, particularly during compound heat and O_3 pollution events similar to the ones examined here. This work highlights the importance of considering both meteorological extremes and regional emission linkages when developing targeted air quality management strategies.

It is noteworthy that although the three episodes analyzed here coincided with Atlantic tropical cyclones, the present case-based analysis does not establish a direct causal relationship between these storms and the frontal evolution or O_3 pollution observed over Oklahoma. Our results directly identify frontal passage, weak prefrontal winds, reduced ventilation, and regional pollutant transport as the proximate meteorological processes contributing to the events. The tropical cyclones should therefore be viewed as part of the broader synoptic context in which these conditions developed. Establishing whether and how Atlantic tropical cyclones systematically modify frontal evolution and regional pollutant transport over the SGP will require analysis of a larger event sample. Future work combining synoptic composites and trajectory analyses with targeted numerical sensitivity experiments could isolate the influence of tropical cyclones on circulation, frontal evolution, and pollutant transport over the region.

In addition, this study highlights both the value and limitations of applying sub-kilometer-scale air quality modeling to real-world events. The innermost WRF-Chem domain (800 m) lies within the turbulence gray zone (Wyngaard, 2004; Zhou et al., 2014), where neither traditional PBL schemes nor LES closures are fully appropriate. Although scale-aware approaches such as the Shin–Hong PBL scheme (Shin & Hong, 2015) used in this study are designed to address this regime, their performance in real-case air quality applications remains insufficiently evaluated. In this context, our results should be interpreted with awareness of these modeling uncertainties. Further systematic assessment of turbulence treatments at gray-zone resolutions is needed to improve confidence in high-resolution simulations of meteorology and air quality (Liu & Zhou, 2022; Takemi &

21698996, 2026, 17, Downloaded from https://agupubs.onlinelibrary.wiley.com/doi/10.1029/2026JD046327 by University Of Oklahoma, Wiley Online Library on [12/10/2026]. See the Terms and Conditions (https://onlinelibrary.wiley.com/terms-and-conditions) on Wiley Online Library for rules of use; OA articles are governed by the applicable Creative Commons License

21698996, 2026, 17, Downloaded from https://agupubs.onlinelibrary.wiley.com/doi/10.1029/2026JD046327 by University Of Oklahoma, Wiley Online Library on [12/10/2026]. See the Terms and Conditions (https://onlinelibrary.wiley.com/terms-and-conditions) on Wiley Online Library for rules of use; OA articles are governed by the applicable Creative Commons License

Rotunno, 2003). Continued development and testing of scale-aware and hybrid turbulence schemes will be important for advancing high-resolution modeling of compound heat and air pollution episodes in complex urban environments (Wang, Zhao, et al., 2025).

Conflict of Interest

The authors declare no conflicts of interest relevant to this study.

Availability Statement

NCEP FNL (Final) operational global analysis and forecast (GFS) data (National Centers for Environmental Prediction, 2015) were downloaded from https://gdex.ucar.edu/datasets/d083003/. The Whole Atmosphere Community Climate Model (WACCM) outputs (Gettelman et al., 2019) were downloaded from https://www.acom.ucar.edu/waccm/download.shtml. The Atmospheric Radiation Measurement (ARM) soundings (Stokes & Schwartz, 1994) were obtained from http://dx.doi.org/10.5439/1021460. The Oklahoma statewide mesoscale observing network (Mesonet) data (Basara et al., 2008; McPherson et al., 2007) were downloaded from http://mesonet.org/ with assistance from Mason Burris. Ozonesondes at National Weather Center in Norman (Auth & Homeyer, 2023) were downloaded from http://weather.ou.edu/~chomeyer/ozsonde_public/. The model configuration, namelists, data-processing and analysis scripts, and simulation outputs produced from this study (Hu, 2026) have been archived at CAPS website https://caps.ou.edu/micronet/HurricaneImpactonO3.html.

Acknowledgments

This work was primarily supported by Grant 20163646499 from the Universidad Nacional de San Agustín de Arequipa (UNSA) of Peru through the LASI Global Change and Human Health Institute and the National Aeronautics and Space Administration (NASA) under Grant 80NSSC24K1056 (Early Career Investigator Program in Earth Science). Financial support for publication was partially provided by the University of Oklahoma Libraries' Open Access Fund. The WRF-Chem simulations were performed on supercomputers Stampede 3 at the Texas Advanced Computing Center (TACC) through allocation TG-ATM160014 from the Advanced Cyberinfrastructure Coordination Ecosystem: Services & Support (ACCESS) program, which is supported by National Science Foundation Grants 2138259, 2138286, 2138307, 2137603, and 2138296. The NEMO development is partially supported by NOAA Weather Program Office (Grant NA22OAR4590512). Dr. Bowen Zhou helped interpret the behavior of different turbulent schemes.

References

Analitis, A., Michelozzi, P., D'Ippoliti, D., de'Donato, F., Menne, B., Matthies, F., et al. (2014). Effects of heat waves on mortality: Effect modification and confounding by air pollutants. *Epidemiology*, *25*(1), 15–22. https://doi.org/10.1097/EDE.0b013e31828ac01b

Auth, R. M., & Homeyer, C. R. (2023). Targeted balloon observations of stratosphere-to-troposphere transport from a mesoscale convective system [Dataset]. *Journal of Geophysical Research: Atmospheres*, *128*(16), e2023JD039139. https://doi.org/10.1029/2023JD039139

Bao, X., Zhang, F., & Sun, J. (2011). Diurnal variations of warm-season precipitation east of the Tibetan Plateau over China. *Monthly Weather Review*, *139*(9), 2790–2810. https://doi.org/10.1175/MWR-D-11-00006.1

Basara, J. B., Hall, P. K., Schroeder, A. J., Illston, B. G., & Nemunaitis, K. L. (2008). Diurnal cycle of the Oklahoma City urban heat island [Dataset]. *Journal of Geophysical Research*, *113*(D20). https://doi.org/10.1029/2008jd010311

Bechtold, P., Kohler, M., Jung, T., Doblas-Reyes, F., Leutbecher, M., Rodwell, M. J., et al. (2008). Advances in simulating atmospheric variability with the ECMWF model: From synoptic to decadal time-scales. *Quarterly Journal of the Royal Meteorological Society*, *134*(634), 1337–1351. https://doi.org/10.1002/qj.289

Beck, H. E., Zimmermann, N. E., McVicar, T. R., Vergopolan, N., Berg, A., & Wood, E. F. (2018). Present and future Köppen-Geiger climate classification maps at 1-km resolution. *Scientific Data*, *5*(1), 180214. https://doi.org/10.1038/sdata.2018.214

Brown, S. S., Dubé, W. P., Karamchandani, P., Yarwood, G., Peischl, J., Ryerson, T. B., et al. (2012). Effects of NOx control and plume mixing on nighttime chemical processing of plumes from coal-fired power plants. *Journal of Geophysical Research*, *117*(D7). https://doi.org/10.1029/2011JD016954

Chen, F., & Dudhia, J. (2001). Coupling an advanced land surface-hydrology model with the Penn State-NCAR MM5 modeling system. Part I: Model implementation and sensitivity. *Monthly Weather Review*, *129*(4), 569–585. https://doi.org/10.1175/1520-0493(2001)129<0569:Caalsh>2.0.Co;2

Choi, Y., & Souri, A. H. (2015). Chemical condition and surface ozone in large cities of Texas during the last decade: Observational evidence from OMI, CAMS, and model analysis. *Remote Sensing of Environment*, *168*, 90–101. https://doi.org/10.1016/j.rse.2015.06.026

Cohan, D. S., Hakami, A., Hu, Y., & Russell, A. G. (2005). Nonlinear response of ozone to emissions: Source apportionment and sensitivity analysis. *Environmental Science & Technology*, *39*(17), 6739–6748. https://doi.org/10.1021/es048664m

Cui, D., Liang, S., Wang, D., & Liu, Z. (2021). A 1 km global dataset of historical (1979–2013) and future (2020–2100) Köppen–Geiger climate classification and bioclimatic variables. *Earth System Science Data*, *13*(11), 5087–5114. https://doi.org/10.5194/essd-13-5087-2021

Daum, P. H., Kleinman, L. I., Springston, S. R., Nunnermacker, L. J., Lee, Y. N., Weinstein-Lloyd, J., et al. (2004). Origin and properties of plumes of high ozone observed during the Texas 2000 air quality study (TexAQS 2000). *Journal of Geophysical Research*, *109*(D17), D17306. https://doi.org/10.1029/2003jd004311

de Gouw, J. A., Parrish, D. D., Frost, G. J., & Trainer, M. (2014). Reduced emissions of CO_2, NOx, and SO_2 from U.S. power plants owing to switch from coal to natural gas with combined cycle technology. *Earth's Future*, *2*(2), 75–82. https://doi.org/10.1002/2013EF000196

Du, H., Yan, M., Liu, X., Zhong, Y., Ban, J., Lu, K., & Li, T. (2024). Exposure to concurrent heatwaves and ozone pollution and associations with mortality risk: A nationwide study in China. *Environmental Health Perspectives*, *132*(4), 47012. https://doi.org/10.1289/ehp13790

Dudhia, J. (1989). Numerical study of convection observed during the winter monsoon experiment using a mesoscale two-dimensional model. *Journal of the Atmospheric Sciences*, *46*(20), 3077–3107. https://doi.org/10.1175/1520-0469(1989)046<3077:Nsocod>2.0.Co;2

EPA. (2025). 2019 emissions modeling platform technical support document. Retrieved from https://www.epa.gov/air-emissions-modeling/2019-emissions-modeling-platform-technical-support-document

Fang, Y., Mauzerall, D. L., Liu, J., Fiore, A. M., & Horowitz, L. W. (2013). Impacts of 21st century climate change on global air pollution-related premature mortality. *Climatic Change*, *121*(2), 239–253. https://doi.org/10.1007/s10584-013-0847-8

Fast, J. D., Gustafson, W. I., Jr., Easter, R. C., Zaveri, R. A., Barnard, J. C., Chapman, E. G., et al. (2006). Evolution of ozone, particulates, and aerosol direct radiative forcing in the vicinity of Houston using a fully coupled meteorology-chemistry-aerosol model. *Journal of Geophysical Research*, *111*(D21). https://doi.org/10.1029/2005jd006721

Feron, S., Cordero, R. R., Damiani, A., Oyola, P., Ansari, T., Pedemonte, J. C., et al. (2023). Compound climate-pollution extremes in Santiago de Chile. *Scientific Reports*, *13*(1), 6726. https://doi.org/10.1038/s41598-023-33890-w

Fibiger, D. L., McDuffie, E. E., Dubé, W. P., Aikin, K. C., Lopez-Hilfiker, F. D., Lee, B. H., et al. (2018). Wintertime overnight NOx removal in a southeastern United States coal-fired power plant plume: A model for understanding winter NOx processing and its implications. *Journal of Geophysical Research: Atmospheres*, *123*(2), 1412–1425. https://doi.org/10.1002/2017JD027768

Fovell, R. G., & Gallagher, A. (2020). Boundary layer and surface verification of the high-resolution rapid refresh, version 3. *Weather and Forecasting*, *35*(6), 2255–2278. https://doi.org/10.1175/waf-d-20-0101.1

Frost, G. J., McKeen, S. A., Trainer, M., Ryerson, T. B., Neuman, J. A., Roberts, J. M., et al. (2006). Effects of changing power plant NOx emissions on ozone in the eastern United States: Proof of concept. *Journal of Geophysical Research*, *111*(D12). https://doi.org/10.1029/2005JD006354

Gamarro, H., Angevine, W. M., McDonald, B. C., Bornstein, R., Ramamurthy, P., Moshary, F., et al. (2026). Simulations of a high ozone episode and heatwave day using a coupled multi-layer urban canopy and chemistry model. *Journal of Geophysical Research: Atmospheres*, *131*(7), e2025JD045552. https://doi.org/10.1029/2025JD045552

Gao, L., Cai, C., & Hu, X.-M. (2022). Air quality prediction using machine learning. In *Machine learning in chemical safety and health* (pp. 267–288).

Gettelman, A., Mills, M. J., Kinnison, D. E., Garcia, R. R., Smith, A. K., Marsh, D. R., et al. (2019). The whole atmosphere community climate model version 6 (WACCM6) [Dataset]. *Journal of Geophysical Research: Atmospheres*, *124*(23), 12380–12403. https://doi.org/10.1029/2019JD030943

Gillani, N. V., & Pleim, J. E. (1996). Sub-grid-scale features of anthropogenic emissions of NOx and VOC in the context of regional eulerian models. *Atmospheric Environment*, *30*(12), 2043–2059. https://doi.org/10.1016/1352-2310(95)00201-4

Goldberg, D. L., Anenberg, S. C., Kerr, G. H., Mohegh, A., Lu, Z., & Streets, D. G. (2021). TROPOMI NO_2 in the United States: A detailed look at the annual averages, weekly cycles, effects of temperature, and correlation with surface NO_2 concentrations. *Earth's Future*, *9*(4), e2020EF001665. https://doi.org/10.1029/2020EF001665

Goldberg, D. L., Tao, M., Kerr, G. H., Ma, S., Tong, D. Q., Fiore, A. M., et al. (2024). Evaluating the spatial patterns of U.S. urban NOx emissions using TROPOMI NO_2. *Remote Sensing of Environment*, *300*, 113917. https://doi.org/10.1016/j.rse.2023.113917

Grell, G. A., Peckham, S. E., Schmitz, R., McKeen, S. A., Frost, G., Skamarock, W. C., & Eder, B. (2005). Fully coupled "online" chemistry within the WRF model. *Atmospheric Environment*, *39*(37), 6957–6975. https://doi.org/10.1016/j.atmosenv.2005.04.027

Guenther, A., Karl, T., Harley, P., Wiedinmyer, C., Palmer, P. I., & Geron, C. (2006). Estimates of global terrestrial isoprene emissions using MEGAN (Model of Emissions of Gases and Aerosols from Nature). *Atmospheric Chemistry and Physics*, *6*(11), 3181–3210. https://doi.org/10.5194/acp-6-3181-2006

Han, Z. S., González-Cruz, J. E., Liu, H. N., Melecio-Vázquez, D., Gamarro, H., Wu, Y. H., et al. (2022). Observed sea breeze life cycle in and around NYC: Impacts on UHI and ozone patterns. *Urban Climate*, *42*, 101109. https://doi.org/10.1016/j.uclim.2022.101109

Hoerling, M., Kumar, A., Dole, R., Nielsen-Gammon, J. W., Eischeid, J., Perlwitz, J., et al. (2013). Anatomy of an extreme event. *Journal of Climate*, *26*(9), 2811–2832. https://doi.org/10.1175/JCLI-D-12-00270.1

Hu, X.-M., Klein, P. M., Xue, M., Lundquist, J. K., Zhang, F., & Qi, Y. (2013). Impact of low-level jets on the nocturnal urban heat island intensity in Oklahoma City. *Journal of Applied Meteorology and Climatology*, *52*(8), 1779–1802. https://doi.org/10.1175/jamc-d-12-0256.1

Hu, X.-M. (2008). *Incorporation of the model of aerosol dynamics, reaction, ionization, and dissolution (MADRID) into the weather research and forecasting model with chemistry (WRF/Chem): Model development and retrospective applications* (PhD thesis). NC State University. Retrieved from http://repository.lib.ncsu.edu/ir/handle/1840.16/5241

Hu, X.-M. (2015). Boundary layer (atmospheric) and air pollution | air pollution meteorology. In G. R. North, J. Pyle, & F. Zhang (Eds.), *Encyclopedia of atmospheric sciences* (2nd ed., pp. 227–236). Academic Press.

Hu, X.-M. (2026). Outputs of WRF-Chem simulations over Oklahoma [Dataset]. Retrieved from https://caps.ou.edu/micronet/HurricaneImpactonO3.html

Hu, X.-M., Crowell, S., Wang, Q., Zhang, Y., Davis, K. J., Xue, M., et al. (2020). Dynamical downscaling of CO_2 in 2016 over the contiguous United States using WRF-VPRM, a weather-biosphere-online-coupled model. *Journal of Advances in Modeling Earth Systems*, *12*(4), e2019MS001875. https://doi.org/10.1029/2019MS001875

Hu, X.-M., Doughty, D. C., Sanchez, K. J., Joseph, E., & Fuentes, J. D. (2012). Ozone variability in the atmospheric boundary layer in Maryland and its implications for vertical transport model. *Atmospheric Environment*, *46*, 354–364. https://doi.org/10.1016/j.atmosenv.2011.09.054

Hu, X.-M., Hu, J., Gao, L., Cai, C., Jiang, Y., Xue, M., et al. (2021). Multisensor and multimodel monitoring and investigation of a wintertime air pollution event ahead of a cold front over eastern China. *Journal of Geophysical Research: Atmospheres*, *126*(10), e2020JD033538. https://doi.org/10.1029/2020jd033538

Hu, X.-M., Klein, P. M., & Xue, M. (2013). Evaluation of the updated YSU planetary boundary layer scheme within WRF for wind resource and air quality assessments. *Journal of Geophysical Research: Atmospheres*, *118*(18), 10490–10505. https://doi.org/10.1002/jgrd.50823

Hu, X.-M., Klein, P. M., Xue, M., Shapiro, A., & Nallapareddy, A. (2013). Enhanced vertical mixing associated with a nocturnal cold front passage and its impact on near-surface temperature and ozone concentration. *Journal of Geophysical Research: Atmospheres*, *118*(7), 2714–2728. https://doi.org/10.1002/jgrd.50309

Hu, X.-M., Klein, P. M., Xue, M., Zhang, F. Q., Doughty, D. C., Forkel, R., et al. (2013). Impact of the vertical mixing induced by low-level jets on boundary layer ozone concentration. *Atmospheric Environment*, *70*, 123–130. https://doi.org/10.1016/j.atmosenv.2012.12.046

Hu, X.-M., Ma, Z., Lin, W., Zhang, H., Hu, J., Wang, Y., et al. (2014). Impact of the Loess Plateau on the atmospheric boundary layer structure and air quality in the North China Plain: A case study. *Science of the Total Environment*, *499*, 228–237. https://doi.org/10.1016/j.scitotenv.2014.08.053

Hu, X.-M., Nielsen-Gammon, J. W., & Zhang, F. Q. (2010). Evaluation of three planetary boundary layer schemes in the WRF model. *Journal of Applied Meteorology and Climatology*, *49*(9), 1831–1844. https://doi.org/10.1175/2010jamc2432.1

Hu, X.-M., Park, J., Supinie, T., Snook, N. A., Xue, M., Brewster, K. A., et al. (2023). Diagnosing near-surface model errors with candidate physics parameterization schemes for the multiphysics rapid refresh forecast system (RRFS) ensemble during winter over the northeastern United States and Southern Great Plains. *Monthly Weather Review*, *151*(1), 39–61. https://doi.org/10.1175/MWR-D-22-0085.1

Hu, X.-M., & Xue, M. (2016). Influence of synoptic sea-breeze fronts on the urban heat island intensity in Dallas–Fort Worth, Texas. *Monthly Weather Review*, *144*(4), 1487–1507. https://doi.org/10.1175/mwr-d-15-0201.1

Hu, X.-M., Xue, M., Klein, P. M., Illston, B. G., & Chen, S. (2016). Analysis of urban effects in Oklahoma City using a dense surface observing network. *Journal of Applied Meteorology and Climatology*, *55*(3), 723–741. https://doi.org/10.1175/JAMC-D-15-0206.1

Hu, X.-M., Xue, M., Kong, F., & Zhang, H. (2019). Meteorological conditions during an ozone episode in Dallas-Fort Worth, Texas, and impact of their modeling uncertainties on air quality prediction. *Journal of Geophysical Research: Atmospheres*, *124*(4), 1941–1961. https://doi.org/10.1029/2018JD029791

21698996, 2026, 17, Downloaded from https://agupubs.onlinelibrary.wiley.com/doi/10.1029/2026JD046327 by University Of Oklahoma, Wiley Online Library on [12/10/2026]. See the Terms and Conditions (https://onlinelibrary.wiley.com/terms-and-conditions) on Wiley Online Library for rules of use; OA articles are governed by the applicable Creative Commons License

Huang, J., Stajner, I., Montuoro, R., Yang, F., Wang, K., Huang, H.-C., et al. (2025). Development of the next-generation air quality prediction system in the Unified Forecast System framework: Enhancing predictability of wildfire air quality impacts. *Bulletin of the American Meteorological Society*. https://doi.org/10.1175/BAMS-D-23-0053.1

Hudak, P. F. (2014). Spatial pattern of ground-level ozone concentration in Dallas-Fort Worth metropolitan area. *International Journal of Environmental Research*, *8*(4), 897–902.

Jacob, D. J., & Winner, D. A. (2009). Effect of climate change on air quality. *Atmospheric Environment*, *43*(1), 51–63. https://doi.org/10.1016/j.atmosenv.2008.09.051

Jiang, G. F., & Fast, J. D. (2004). Modeling the effects of VOC and NOX emission sources on ozone formation in Houston during the TexAQS 2000 field campaign. *Atmospheric Environment*, *38*(30), 5071–5085. https://doi.org/10.1016/j.atmosenv.2004.06.012

Jiménez, P. A., Dudhia, J., González-Rouco, J. F., Navarro, J., Montávez, J. P., & García-Bustamante, E. (2012). A revised scheme for the WRF surface layer formulation. *Monthly Weather Review*, *140*(3), 898–918. https://doi.org/10.1175/mwr-d-11-00056.1

Jin, X., Yang, Y., Gonzalez Abad, G., Nowlan, C., & Liu, X. (2025). Observing the diurnal variations of Ozone-NOx-VOC chemistry over the U.S. from the geostationary TEMPO instrument. *Geophysical Research Letters*, *52*(14), e2025GL116394. https://doi.org/10.1029/2025GL116394

Jin, X. M., Fiore, A., Boersma, K. F., De Smedt, I., & Valin, L. (2020). Inferring changes in summertime surface Ozone-NOx-VOC chemistry over US urban areas from two decades of satellite and ground-based observations. *Environmental Science & Technology*, *54*(11), 6518–6529. https://doi.org/10.1021/acs.est.9b07785

Kiesewetter, G., Borken-Kleefeld, J., Schöpp, W., Heyes, C., Thunis, P., Bessagnet, B., et al. (2015). Modelling street level PM_{10} concentrations across Europe: Source apportionment and possible futures. *Atmospheric Chemistry and Physics*, *15*(3), 1539–1553. https://doi.org/10.5194/acp-15-1539-2015

Kim, S., Byun, D. W., & Cohan, D. (2009). Contributions of inter- and intra-state emissions to ozone over Dallas-Fort Worth, Texas. *Civil Engineering and Environmental Systems*, *26*(1), 103–116. https://doi.org/10.1080/10286600802005364

Kim, S.-W., Heckel, A., Frost, G. J., Richter, A., Gleason, J., Burrows, J. P., et al. (2009). NO_2 columns in the western United States observed from space and simulated by a regional chemistry model and their implications for NOx emissions. *Journal of Geophysical Research*, *114*(D11). https://doi.org/10.1029/2008JD011343

Kim, S. W., McKeen, S. A., Frost, G. J., Lee, S. H., Trainer, M., Richter, A., et al. (2011). Evaluations of NO_x and highly reactive VOC emission inventories in Texas and their implications for ozone plume simulations during the Texas Air Quality Study 2006. *Atmospheric Chemistry and Physics*, *11*(22), 11361–11386. https://doi.org/10.5194/acp-11-11361-2011

Klein, P. M., Hu, X.-M., Shapiro, A., & Xue, M. (2015). Linkages between boundary-layer structure and the development of nocturnal low-level jets in central Oklahoma. *Boundary-Layer Meteorology*, *158*(3), 1–26. https://doi.org/10.1007/s10546-015-0097-6

Klein, P. M., Hu, X.-M., & Xue, M. (2014). Impacts of mixing processes in nocturnal atmospheric boundary layer on urban ozone concentrations. *Boundary-Layer Meteorology*, *150*(1), 107–130. https://doi.org/10.1007/s10546-013-9864-4

Klein, P. M., Lundquist, J. K., & Basara, J. B. (2010). Mixing processes in the nocturnal atmospheric boundary layer and their impacts on urban ozone concentrations and heat island intensity. In *The 19th Symposium on Boundary Layers and Turbulence/29th Conference on Agricultural and Forest Meteorology/9th Symposium on the Urban Environment*.

Koster, R. D., Dirmeyer, P. A., Guo, Z., Bonan, G., Chan, E., Cox, P., et al. (2004). Regions of strong coupling between soil moisture and precipitation. *Science*, *305*(5687), 1138–1140. https://doi.org/10.1126/science.1100217

Langford, A. O., Senff, C. J., Alvarez, R. J., Banta, R. M., Hardesty, R. M., Parrish, D. D., & Ryerson, T. B. (2011). Comparison between the TOPAZ airborne ozone LiDAR and in situ measurements during TexAQS 2006. *Journal of Atmospheric and Oceanic Technology*, *28*(10), 1243–1257. https://doi.org/10.1175/Jtech-D-10-05043.1

Lau, N.-C., & Nath, M. J. (2012). A model study of heat waves over North America: Meteorological aspects and projections for the twenty-first century. *Journal of Climate*, *25*(14), 4761–4784. https://doi.org/10.1175/JCLI-D-11-00575.1

Lawal, A. S., Russell, A. G., & Kaiser, J. (2022). Assessment of airport-related emissions and their impact on air quality in Atlanta, GA, using CMAQ and TROPOMI. *Environmental Science & Technology*, *56*(1), 98–108. https://doi.org/10.1021/acs.est.1c03388

Lee, E., Bieda, R., Shanmugasundaram, J., & Basara Richter, H. (2016). Land surface and atmospheric conditions associated with heat waves over the Chickasaw Nation in the South Central United States. *Journal of Geophysical Research: Atmospheres*, *121*(11), 6284–6298. https://doi.org/10.1002/2015JD024659

Lee, P., McQueen, J., Stajner, I., Huang, J., Pan, L., Tong, D., et al. (2017). NAQFC developmental forecast guidance for fine particulate matter (PM2.5). *Weather and Forecasting*, *32*(1), 343–360. https://doi.org/10.1175/WAF-D-15-0163.1

Leffel, J., Wang, C., Hu, X.-M., Feron, S., & Henry, S. (2025). Cities as hotspots of compound heat and fine particulate matter pollution: A 23-year urban–rural comparison across the United States. *Environmental Research*, *285*, 122508. https://doi.org/10.1016/j.envres.2025.122508

Lei, R., Talbot, R., Wang, Y., Wang, S.-C., & Estes, M. (2019). Surface MDA8 ozone variability during cold front events over the contiguous United States during 2003–2017. *Atmospheric Environment*, *213*, 359–366. https://doi.org/10.1016/j.atmosenv.2019.06.003

Lei, R. X., Talbot, R., Wang, Y. X., Wang, S. C., & Estes, M. (2018). Influence of cold fronts on variability of daily surface O-3 over the Houston-Galveston-Brazoria Area in Texas USA during 2003-2016. *Atmosphere*, *9*(5), 159. https://doi.org/10.3390/atmos9050159

Li, M., McDonald, B. C., McKeen, S. A., Eskes, H., Levelt, P., Francoeur, C., et al. (2021). Assessment of updated fuel-based emissions inventories over the contiguous United States using TROPOMI NO_2 retrievals. *Journal of Geophysical Research: Atmospheres*, *126*(24), e2021JD035484. https://doi.org/10.1029/2021JD035484

Liu, M., & Zhou, B. (2022). Variations of subgrid-scale turbulent fluxes in the dry convective boundary layer at gray zone resolutions. *Journal of the Atmospheric Sciences*, *79*(12), 3245–3261. https://doi.org/10.1175/JAS-D-22-0085.1

Liu, Y., Chen, F., Warner, T., & Basara, J. (2006). Verification of a mesoscale data-assimilation and forecasting system for the Oklahoma City area during the joint urban 2003 field project. *Journal of Applied Meteorology and Climatology*, *45*(7), 912–929. https://doi.org/10.1175/JAM2383.1

Louis, J. F. (1979). Parametric model of vertical eddy fluxes in the atmosphere. *Boundary-Layer Meteorology*, *17*(2), 187–202. https://doi.org/10.1007/Bf00117978

Luria, M., Valente, R. J., Bairai, S., Parkhurst, W. J., & Tanner, R. L. (2008). Airborne study of ozone formation over Dallas, Texas. *Atmospheric Environment*, *42*(29), 6951–6958. https://doi.org/10.1016/j.atmosenv.2008.04.057

Ma, S., Liu, F., Xing, J., Baek, B. H., Wang, C.-T., Li, Y., et al. (2025). Timely updates of anthropogenic emission with satellite and ground observations: Comparison of multiple top-down methods against bottom-up national emission inventories. *Journal of Geophysical Research: Atmospheres*, *130*(22), e2025JD044157. https://doi.org/10.1029/2025JD044157

Ma, S., & Tong, D. Q. (2022). Neighborhood emission mapping operation (NEMO): A 1-km anthropogenic emission dataset in the United States. *Scientific Data*, *9*(1), 680. https://doi.org/10.1038/s41597-022-01790-9

21698996, 2026, 17, Downloaded from https://agupubs.onlinelibrary.wiley.com/doi/10.1029/2026JD046327 by University Of Oklahoma, Wiley Online Library on [12/10/2026]. See the Terms and Conditions (https://onlinelibrary.wiley.com/terms-and-conditions) on Wiley Online Library for rules of use; OA articles are governed by the applicable Creative Commons License

McDonald, B. C., de Gouw, J. A., Gilman, J. B., Jathar, S. H., Akherati, A., Cappa, C. D., et al. (2018). Volatile chemical products emerging as largest petrochemical source of urban organic emissions. *Science*, *359*(6377), 760–764. https://doi.org/10.1126/science.aaq0524

McNider, R. T., Pour-Biazar, A., Doty, K., White, A., Wu, Y., Qin, M., et al. (2018). Examination of the physical atmosphere in the Great Lakes Region and its potential impact on air quality—Over-water stability and satellite assimilation. *Journal of Applied Meteorology and Climatology*, *57*(12), 2789–2816. https://doi.org/10.1175/jamc-d-17-0355.1

McPherson, R. A., Fiebrich, C. A., Crawford, K. C., Elliott, R. L., Kilby, J. R., Grimsley, D. L., et al. (2007). Statewide monitoring of the mesoscale environment: A technical update on the Oklahoma Mesonet [Dataset]. *Journal of Atmospheric and Oceanic Technology*, *24*(3), 301–321. https://doi.org/10.1175/Jtech1976.1

Meng, X., Wang, W., Shi, S., Zhu, S., Wang, P., Chen, R., et al. (2022). Evaluating the spatiotemporal ozone characteristics with high-resolution predictions in mainland China, 2013–2019. *Environmental Pollution*, *299*, 118865. https://doi.org/10.1016/j.envpol.2022.118865

Mlawer, E. J., Taubman, S. J., Brown, P. D., Iacono, M. J., & Clough, S. A. (1997). Radiative transfer for inhomogeneous atmospheres: RRTM, a validated correlated-k model for the longwave. *Journal of Geophysical Research*, *102*(D14), 16663–16682. https://doi.org/10.1029/97jd00237

Morris, G. A., Ford, B., Rappenglück, B., Thompson, A. M., Mefferd, A., Ngan, F., & Lefer, B. (2010). An evaluation of the interaction of morning residual layer and afternoon mixed layer ozone in Houston using ozonesonde data. *Atmospheric Environment*, *44*(33), 4024–4034. https://doi.org/10.1016/j.atmosenv.2009.06.057

Namias, J. (1982). Anatomy of Great Plains Protracted Heat Waves (especially the 1980 U.S. summer drought). *Monthly Weather Review*, *110*(7), 824–838. https://doi.org/10.1175/1520-0493(1982)110<0824:AOGPPH>2.0.CO;2

National Centers for Environmental Prediction. (2015). NCEP GDAS/FNL 0.25 degree global tropospheric analyses and forecast grids [Dataset]. https://doi.org/10.5065/D65Q4T4Z

Nunnermacker, L. J., Kleinman, L. I., Imre, D., Daum, P. H., Lee, Y.-N., Lee, J. H., et al. (2000). NOy lifetimes and O_3 production efficiencies in urban and power plant plumes: Analysis of field data. *Journal of Geophysical Research*, *105*(D7), 9165–9176. https://doi.org/10.1029/1999JD900753

Parrish, D. D., Allen, D. T., Bates, T. S., Estes, M., Fehsenfeld, F. C., Feingold, G., et al. (2009). Overview of the second Texas air quality study (TexAQS II) and the Gulf of Mexico atmospheric composition and climate study (GoMACCS). *Journal of Geophysical Research*, *114*(D7). https://doi.org/10.1029/2009jd011842

Perkins-Kirkpatrick, S. E., & Lewis, S. C. (2020). Increasing trends in regional heatwaves. *Nature Communications*, *11*(1), 3357. https://doi.org/10.1038/s41467-020-16970-7

Pongprueksa, P. (2013). Application of satellite data in a regional model to improve long-term ozone simulations. *Journal of Atmospheric Chemistry*, *70*(4), 317–340. https://doi.org/10.1007/s10874-013-9270-9

Qian, T., Zhao, P., Zhang, F., & Bao, X. (2015). Rainy-season precipitation over the Sichuan Basin and adjacent regions in southwestern China. *Monthly Weather Review*, *143*(1), 383–394. https://doi.org/10.1175/MWR-D-13-00158.1

Qin, Y., Walk, T., Gary, R., Yao, X., & Elles, S. (2007). C-2-C-10 nonmethane hydrocarbons measured in Dallas, USA - Seasonal trends and diurnal characteristics. *Atmospheric Environment*, *41*(28), 6018–6032. https://doi.org/10.1016/j.atmosenv.2007.03.008

Ramsey, N. R., Klein, P. M., & Moore, B. (2014). The impact of meteorological parameters on urban air quality. *Atmospheric Environment*, *86*, 58–67. https://doi.org/10.1016/j.atmosenv.2013.12.006

Rozhina, E., Ishmukhametov, I., Nigamatzyanova, L., Akhatova, F., Batasheva, S., Taskaev, S., et al. (2021). Comparative toxicity of fly ash: An in vitro study. *Molecules*, *26*(7), 1926. https://doi.org/10.3390/molecules26071926

Sandu, A., Daescu, D. N., & Carmichael, G. R. (2003). Direct and adjoint sensitivity analysis of chemical kinetic systems with KPP: Part I—Theory and software tools. *Atmospheric Environment*, *37*(36), 5083–5096. https://doi.org/10.1016/j.atmosenv.2003.08.019

Sather, M. E., & Cavender, K. (2012). Update of long-term trends analysis of ambient 8-hour ozone and precursor monitoring data in the South Central U.S.; encouraging news. *Journal of Environmental Monitoring*, *14*(2), 666–676. https://doi.org/10.1039/c2em10862c

Seneviratne, S. I., Corti, T., Davin, E. L., Hirschi, M., Jaeger, E. B., Lehner, I., et al. (2010). Investigating soil moisture–climate interactions in a changing climate: A review. *Earth-Science Reviews*, *99*(3), 125–161. https://doi.org/10.1016/j.earscirev.2010.02.004

Senff, C. J., Alvarez, R. J., Hardesty, R. M., Banta, R. M., & Langford, A. O. (2010). Airborne LiDAR measurements of ozone flux downwind of Houston and Dallas. *Journal of Geophysical Research*, *115*(D20), D20307. https://doi.org/10.1029/2009jd013689

Senff, C. J., Hardesty, R. M., Alvarez, R. J., II., & Mayor, S. D. (1998). Airborne LiDAR characterization of power plant plumes during the 1995 Southern Oxidants Study. *Journal of Geophysical Research*, *103*(D23), 31173–31189. https://doi.org/10.1029/98JD02625

Shapiro, J. S. (2022). Pollution trends and US environmental policy: Lessons from the past half century. *Review of Environmental Economics and Policy*, *16*(1), 42–61. https://doi.org/10.1086/718054

Shen, C., Shen, A., Cui, Y., Chen, X., Liu, Y., Fan, Q., et al. (2022). Spatializing the roughness length of heterogeneous urban underlying surfaces to improve the WRF simulation-part 1: A review of morphological methods and model evaluation. *Atmospheric Environment*, *270*, 118874. https://doi.org/10.1016/j.atmosenv.2021.118874

Shin, H. H., & Hong, S. Y. (2015). Representation of the subgrid-scale turbulent transport in convective boundary layers at gray-zone resolutions. *Monthly Weather Review*, *143*(1), 250–271. https://doi.org/10.1175/Mwr-D-14-00116.1

Sillman, S. (1999). The relation between ozone, NOx and hydrocarbons in urban and polluted rural environments. *Atmospheric Environment*, *33*(12), 1821–1845. https://doi.org/10.1016/S1352-2310(98)00345-8

Skamarock, W. C., & Klemp, J. B. (2008). A time-split nonhydrostatic atmospheric model for weather research and forecasting applications. *Journal of Computational Physics*, *227*(7), 3465–3485. https://doi.org/10.1016/j.jcp.2007.01.037

Stockwell, W. R., Kirchner, F., Kuhn, M., & Seefeld, S. (1997). A new mechanism for regional atmospheric chemistry modeling. *Journal of Geophysical Research*, *102*(D22), 25847–25879. https://doi.org/10.1029/97jd00849

Stokes, G. M., & Schwartz, S. E. (1994). The atmospheric radiation measurement (ARM) program: Programmatic background and design of the cloud and radiation test bed [Dataset]. *Bulletin of the American Meteorological Society*, *75*(7), 1201–1222. https://doi.org/10.1175/1520-0477(1994)075<1201:TARMPP>2.0.CO;2

Sumner, P. (2025). *Assessing the Dallas-Fort Worth urban microclimate and surface ozone variability under differing drought conditions*. University of Texas at Arlington. Retrieved from https://mavmatrix.uta.edu/ees_theses/216

Takemi, T., & Rotunno, R. (2003). The effects of subgrid model mixing and numerical filtering in simulations of mesoscale cloud systems. *Monthly Weather Review*, *131*(9), 2085–2101. https://doi.org/10.1175/1520-0493(2003)131<2085:TEOSMM>2.0.CO;2

Teng, H., Branstator, G., Meehl, G. A., & Washington, W. M. (2016). Projected intensification of subseasonal temperature variability and heat waves in the Great Plains. *Geophysical Research Letters*, *43*(5), 2165–2173. https://doi.org/10.1002/2015GL067574

Thornton, P. E., Shrestha, R., Thornton, M., Kao, S.-C., Wei, Y., & Wilson, B. E. (2021). Gridded daily weather data for North America with comprehensive uncertainty quantification. *Scientific Data*, *8*(1), 190. https://doi.org/10.1038/s41597-021-00973-0

21698996, 2026, 17, Downloaded from https://agupubs.onlinelibrary.wiley.com/doi/10.1029/2026JD046327 by University Of Oklahoma, Wiley Online Library on [12/10/2026]. See the Terms and Conditions (https://onlinelibrary.wiley.com/terms-and-conditions) on Wiley Online Library for rules of use; OA articles are governed by the applicable Creative Commons License

Trainer, M., Ridley, B. A., Buhr, M. P., Kok, G., Walega, J., Hübler, G., et al. (1995). Regional ozone and urban plumes in the southeastern United States: Birmingham, A case study. *Journal of Geophysical Research*, *100*(D9), 18823–18834. https://doi.org/10.1029/95JD01641

Van Dingenen, R., Dentener, F., Crippa, M., Leitao, J., Marmer, E., Rao, S., et al. (2018). TM5-FASST: A global atmospheric source–receptor model for rapid impact analysis of emission changes on air quality and short-lived climate pollutants. *Atmospheric Chemistry and Physics*, *18*(21), 16173–16211. https://doi.org/10.5194/acp-18-16173-2018

Wang, C., Hu, X.-M., Feron, S., Leffel, J., & Cordero, R. R. (2025). Compound heat and ozone pollution in the urban environment. *Urban Climate*, *62*, 102511. https://doi.org/10.1016/j.uclim.2025.102511

Wang, C., Zhao, Y., Li, Q., Wang, Z.-H., & Fan, J. (2025). Ultrafine-resolution urban climate modeling: Resolving processes across scales. *Journal of Advances in Modeling Earth Systems*, *17*(6), e2025MS005053. https://doi.org/10.1029/2025MS005053

Wang, J., Xiao, X., Qin, Y., Dong, J., Zhang, G., Yang, X., et al. (2024). Annual maps of forest and evergreen forest in the contiguous United States during 2015–2017 from analyses of PALSAR-2 and Landsat images. *Earth System Science Data*, *16*(10), 4619–4639. https://doi.org/10.5194/essd-16-4619-2024

Wert, B. P., Trainer, M., Fried, A., Ryerson, T. B., Henry, B., Potter, W., et al. (2003). Signatures of terminal alkene oxidation in airborne formaldehyde measurements during TexAQS 2000. *Journal of Geophysical Research*, *108*(D3), 4104. https://doi.org/10.1029/2002jd002502

World Health Organization. (2021). *WHO global air quality guidelines: Particulate matter (PM2.5 and PM10), ozone, nitrogen dioxide, sulfur dioxide and carbon monoxide*. World Health Organization.

Wyngaard, J. C. (2004). Toward numerical modeling in the "Terra Incognita". *Journal of the Atmospheric Sciences*, *61*(14), 1816–1826. https://doi.org/10.1175/1520-0469(2004)061<1816:tnmitt>2.0.co;2

Xing, J., Baek, B. H., Li, S., Wang, C.-T., Song, G., Ma, S., et al. (2024). A physically constrained deep-learning fusion method for estimating surface NO_2 concentration from satellite and ground monitors. *Environmental Science & Technology*, *58*(48), 21218–21228. https://doi.org/10.1021/acs.est.4c07341

Yang, Z., Dominguez, F., & Zeng, X. (2019). Large and local-scale features associated with heat waves in the United States in reanalysis products and the NARCCAP model ensemble. *Climate Dynamics*, *52*(3), 1883–1901. https://doi.org/10.1007/s00382-018-4414-x

Ye, D. (1981). Some characteristics of the summer circulation over the Qinghai-Xizang (Tibet) Plateau and its neighborhood. *Bulletin of the American Meteorological Society*, *62*(1), 14–19. https://doi.org/10.1175/1520-0477(1981)062<0014:SCOTSC>2.0.CO;2

Yu, S. C., Eder, B., Dennis, R., Chu, S. H., & Schwartz, S. E. (2006). New unbiased symmetric metrics for evaluation of air quality models. *Atmospheric Science Letters*, *7*(1), 26–34. https://doi.org/10.1002/asl.125

Yu, S. C., Mathur, R., Pleim, J., Pouliot, G., Wong, D., Eder, B., et al. (2012). Comparative evaluation of the impact of WRF-NMM and WRF-ARW meteorology on CMAQ simulations for O-3 and related species during the 2006 TexAQS/GoMACCS campaign. *Atmospheric Pollution Research*, *3*(2), 149–162. https://doi.org/10.5094/Apr.2012.015

Zhang, H., Li, J., Ying, Q., Guven, B. B., & Olaguer, E. P. (2013). Source apportionment of formaldehyde during TexAQS 2006 using a source-oriented chemical transport model. *Journal of Geophysical Research: Atmospheres*, *118*(3), 1525–1535. https://doi.org/10.1002/jgrd.50197

Zhang, H., & Ying, Q. (2011). Contributions of local and regional sources of NOx to ozone concentrations in Southeast Texas. *Atmospheric Environment*, *45*(17), 2877–2887. https://doi.org/10.1016/j.atmosenv.2011.02.047

Zhang, J., & Rao, S. T. (1999). The role of vertical mixing in the temporal evolution of ground-level ozone concentrations. *Journal of Applied Meteorology*, *38*(12), 1674–1691. https://doi.org/10.1175/1520-0450(1999)038<1674:TROVMI>2.0.CO;2

Zhou, B., Simon, J. S., & Chow, F. K. (2014). The convective boundary layer in the Terra Incognita. *Journal of the Atmospheric Sciences*, *71*(7), 2545–2563. https://doi.org/10.1175/JAS-D-13-0356.1

Zhu, J. H., & Liang, X. Z. (2013). Impacts of the Bermuda high on regional climate and ozone over the United States. *Journal of Climate*, *26*(3), 1018–1032. https://doi.org/10.1175/Jcli-D-12-00168.1

Zscheischler, J., Martius, O., Westra, S., Bevacqua, E., Raymond, C., Horton, R. M., et al. (2020). A typology of compound weather and climate events. *Nature Reviews Earth & Environment*, *1*(7), 333–347. https://doi.org/10.1038/s43017-020-0060-z

21698996, 2026, 17, Downloaded from https://agupubs.onlinelibrary.wiley.com/doi/10.1029/2026JD046327 by University Of Oklahoma, Wiley Online Library on [12/10/2026]. See the Terms and Conditions (https://onlinelibrary.wiley.com/terms-and-conditions) on Wiley Online Library for rules of use; OA articles are governed by the applicable Creative Commons License